

Associated Material

Supporting Information

Organophosphonate- and dimethylarsinate-functionalized hexamolybdates(V) and their solution and gas phase properties

Vinaya Siby,^a Arun Pal,^a Bassem S. Bassil,^a Saurav Bhattacharya,^a Anusree Sundar,^a Juliane Oberstein,^a Damin Kim,^a Rizul Gupta,^a Alisher Kuanysh,^a Jana Hölscher,^a Dorothea Schmidt,^a Nikolai Kuhnert,^a Ulrich Kortz^{a*}

^a *School of Science, Constructor University, Campus Ring 1, 28759 Bremen, Germany, Email: ukortz@constructor.university*

Materials and physical measurements: All reagents were used as purchased without further purification. The hetero groups (4-fluorophenyl) phosphonic acid (L_{PF}) and (4-trifluoromethoxyphenyl) phosphonic acid (L_{POCF_3}) were synthesized by slightly modifying the literature procedures (see Exp. Section for details, structures depicted in Figures S1-S2). The infrared (FT-IR) spectra of the samples in the solid state were recorded using KBr discs on a Nicolet Avatar 370 spectrophotometer ($400\text{--}4000\text{ cm}^{-1}$) with 32 scans and 4 cm^{-1} resolution. The peak intensities are abbreviated as follows: w, weak; m, medium; s, strong; sh, shoulder. Thermogravimetric analysis (TGA) was conducted on TA Instrument SDT Q600 ramped from room temperature to $600\text{ }^\circ\text{C}$ at a heating rate of $5\text{ }^\circ\text{C}/\text{min}$ in N_2 atmosphere to determine the crystal water content. The multinuclear solution NMR spectra were acquired using a JEOL ECS 400 MHz spectrometer equipped with a 5-mm probe. Chemical shift values were referenced to tetramethyl silane (^{13}C and ^1H), 85% H_3PO_4 (^{31}P), and CFCl_3 (^{19}F). The instrument was tuned to resonance frequencies of 399.78 MHz, 100.52 MHz, 161.83 MHz and 376.17 MHz for ^1H , ^{13}C , ^{31}P and ^{19}F NMR, respectively. The elemental analyses were carried out by Zentrallabor, Technische Universität Hamburg (TUHH), Am Schwarzenberg-Campus 1, 21073 Hamburg (Na, Mo, P, and As) and Analytische Laboratorien, Industriepark Kaiserau (Haus Heidbruch), 51789 Lindlar, (Germany) and Carl von Ossietzky University Oldenburg, 26129 Oldenburg (Germany) (CHN). The Na analysis was further verified in house by atomic absorption (AA) spectroscopy

using a Varian SpectrAA 220 AA spectrometer. Powder X-ray diffraction (PXRD) patterns were obtained utilizing a Rigaku Miniflex 600 (Rigaku Corporation, Tokyo, Japan) employing a primary beam Cu K α radiation ($\lambda = 1.541838 \text{ \AA}$) at 40 kV and 15 mA. The scan range spanned 2θ angles from 3 to 50° incrementally measured in steps of 0.01°, with a scan rate of 10° min⁻¹. The synthesis of the hetero groups L_{POCF₃} and L_{PF} was carried out in 30 ml pressure vials using a CEM Discover SP microwave reactor (CEM Microwave Technology Ltd., Buckingham, UK) under microwave radiation. High-resolution mass spectra were recorded using a Bruker Daltonics QTOF Impact HD mass spectrometer employing both negative and positive electrospray ionization modes. The QTOF Impact mass spectrometer (Bruker Daltonics) was fitted with an ESI source and external calibration was achieved with 10 mL of 0.1M sodium formate solution. The instrument ion source and the tubing were rinsed with methanol. The calibration was carried out using the enhanced quadratic calibration mode. All MS measurements were performed in both negative and positive ion modes. Samples were measured as direct infusions at a concentration of 10 $\mu\text{g/mL}$ in deionized water at a flow rate of 180 $\mu\text{L/min}$. Samples were prepared by dissolving 1 mg of POM in 1 mL of deionized water followed by a 1:100 dilution. Spectral simulations were carried out in Data Analysis 4.1 (Bruker Daltonics, Bremen).

Ion mobility mass spectrometry: Solid samples of NaNH₄-CH₃PMo₆ and Na-Mo₇ were resuspended at 1 mg of solid per 100 μL of methanol which resulted in partial solubilization. Both samples were subjected to vortexing for approximately 2 minutes, and then centrifuged at 2000 g for 2 minutes. 100 μL was aspirated from each sample and diluted 1:10 with methanol (v/v) prior to infusion. Ion mobility experiments were carried out using SELECT SERIES Cyclic IMS tuning and acquisition parameters: Samples were infused at a flow rate of 10 $\mu\text{L/min}$ via a standard flow ESI source with the instrument operating in negative ion mode. The capillary voltage was 1.60 kV, with desolvation gas flow and temperature at 800 L/hr and 400 °C, respectively. The source temperature was 100 °C, and the cone voltage 80 V. The instrument was operated using a mass range of 50 to 2000 m/z , with the time-of-flight mass analyser operated in V-mode. The ion mobility was performed using a single pass of the cyclic mobility device: the traveling wave height propagating the ion separation was set to 24 V, the traveling wave velocity to 375 m/s, data were acquired as two TOF pushes per one mobility data bin, ADC detector start delay was offset automatically and data were acquired for 1 minute per sample at a scan duration of 0.5 s.

X-ray Crystallography: Data for $\text{NaNH}_4\text{-PMo}_6$ were collected at 100 K on a Bruker D8 SMART APEX II CCD diffractometer with kappa geometry and a graphite monochromator ($\text{Mo K}\alpha$ radiation, $\lambda = 0.71073 \text{ \AA}$) by using the APEX III software package. [1] The collected data underwent cell refinement and data reduction using SAINT, [2] with multi-scan absorption corrections performed by SADABS. [2] Structure solution was achieved through direct methods utilizing successive difference Fourier maps with SHELXS-97, [3] followed by refinement on F2 using SHELXL-2014. [4] Anisotropic thermal parameters were applied to refine all non-hydrogen atoms. For Na-HPMo_6 , $\text{NaNH}_4\text{-CH}_3\text{PMo}_6$, $\text{NaNH}_4\text{-HO}_2\text{CCH}_2\text{PMo}_6$, $\text{Na-HO}_2\text{CC}_2\text{H}_4\text{PMo}_6\cdot\text{dmsO}$, $\text{NaNH}_4\text{-C}_6\text{H}_5\text{PMo}_6$, $\text{NaNH}_4\text{-FC}_6\text{H}_4\text{PMo}_6$, $\text{NaNH}_4\text{-F}_3\text{COC}_6\text{H}_4\text{PMo}_6$, Na-Mo_7 , indexing and data collection were conducted using a Rigaku XtaLAB Synergy Dualflex HyPix single-crystal diffractometer with kappa geometry and a graphite monochromator ($\lambda_{\text{Mo K}\alpha} = 0.71073 \text{ \AA}$), operated via the CrysAlisPro software package. [5] Empirical absorption corrections were performed using ABSPACK program. [6] Structure solution was achieved through direct methods utilizing successive difference Fourier maps, and refinements were carried out against all data using SHELXL-2014. [4] Anisotropic refinement was applied to non-hydrogen atoms, and refinements were performed via full-matrix least squares against $|F|$. Crystal structure images were generated using Diamond, version 3.2 (software copyright, Crystal Impact GbR). All measurements were conducted with crystals mounted on Hampton cryoloops with paratone-N oil at 100 K. The crystal structures of $\text{NaNH}_4\text{-HO}_2\text{CCH}_2\text{PMo}_6$, $\text{NaNH}_4\text{-C}_6\text{H}_5\text{PMo}_6$, $\text{NaNH}_4\text{-FC}_6\text{H}_4\text{PMo}_6$ and $\text{NaNH}_4\text{-F}_3\text{COC}_6\text{H}_4\text{PMo}_6$ displayed various levels of disorder within the phosphonate organic groups. The crystal structure of $\text{Na-HO}_2\text{CC}_2\text{H}_4\text{PMo}_6\cdot\text{dmsO}$ was obtained upon recrystallization of the compound from an NMR tube with DMSO as solvent. The corresponding CIF files can be obtained free of charge from <https://www.ccdc.cam.ac.uk/structures/>, deposition numbers 2394921-2394926 and 2406188-2406190.

Bond Valence Sum Calculations: The bond valence sum (BVS) calculations for the molybdenum and oxygen atoms (Tables S2-S10) were performed on a program copyrighted by Chris Hormillosa & Sean Healy and distributed by I. D. Brown. [7]

FT-IR spectra: The IR spectra (Figure S3-S8) ascertain the structural similarities of the polyanions within the fingerprint region from 1200 to 400 cm^{-1} . The bands at 3400-3000 cm^{-1} and 1640-1620 cm^{-1} correspond to $\nu_{as}[\text{O-H}]$ and $\delta[\text{O-H}]$ vibrations of the interstitial water molecules, while the two weak peaks in the 3030-2800 cm^{-1} region and medium intense bands near 1404 cm^{-1}

belong to $\nu_{as}[\text{C-H}]$ and $\delta[\text{C-H}]$ vibrations of methyl groups in the dimethylarsinate ligands. Furthermore, the broad peaks in the 3600-3400 cm^{-1} region indicate the stretching vibrations of the NH_4^+ group. The presence of NH_4^+ as counter cations in the clusters is confirmed by elemental analysis. The characteristic bands at 980-850 cm^{-1} and 600-400 cm^{-1} can be attributed to $\nu_{as}[\text{Mo=O}]$ and $\nu_{as}[\text{Mo-O(Mo)}]$ bond stretching vibrations. The $\nu_{as}[\text{As-O}]$ vibration mode appears as a strong band at 820-825 cm^{-1} with shoulders at 849-857 cm^{-1} and the $\nu_{as}[\text{As-C}]$ vibration mode occurs at 1274-1278 cm^{-1} as peaks of medium intensity with shoulders at 1254-1259 cm^{-1} . The bands at 1444-1274 cm^{-1} and 1143-1010 cm^{-1} correspond to $\nu_{as}[\text{P-C}]$ and $\nu_{as}[\text{P-O}]$ stretching vibrations of the heteropolymolybdates and the bands at 1581 and 1559 cm^{-1} pertain to carbonyl stretching frequencies of the carboxylate groups in $\text{NaNH}_4\text{-HO}_2\text{CCH}_2\text{PMo}_6$ and $\text{NaNH}_4\text{-HO}_2\text{CC}_2\text{H}_4\text{PMo}_6$ (Figure S5), respectively, indicating the incorporation of the phosphonocarboxylate moieties in the polyanion. Additionally, the bands at 1500-1400 cm^{-1} in $\text{NaNH}_4\text{-C}_6\text{H}_5\text{PMo}_6$ (Figure S4), $\text{NaNH}_4\text{-FC}_6\text{H}_4\text{PMo}_6$ (Figure S6), and $\text{NaNH}_4\text{-F}_3\text{COC}_6\text{H}_4\text{PMo}_6$ (Figure S7) can be attributed to their respective asymmetric $\nu_{as}[\text{C-F}]$ and $\nu_{as}[\text{C=C}]$ stretching vibrations. The presence of a single sharp band at 969 cm^{-1} for **Na-Mo₇** (Figure S8) in comparison to the two strong bands at 957 and 920 cm^{-1} for $\text{NaNH}_4\text{-PMo}_6$ for $\nu_{as}[\text{Mo=O}]$ indicate a higher symmetry for the isopolymolybdate ion.

Thermogravimetric Analysis: The thermograms of the freshly prepared and air-dried samples initiated with a dehydration step due to the loss of interstitial water molecules (calc(found)%): $\text{NaNH}_4\text{-PMo}_6$, 6.0(6.9); **Na-HPMo₆**, 10.9(11.8); $\text{NaNH}_4\text{-CH}_3\text{PMo}_6$, 13.2(12.7); $\text{NaNH}_4\text{-HO}_2\text{CCH}_2\text{PMo}_6$, 13.0(9.9); $\text{NaNH}_4\text{-HO}_2\text{CC}_2\text{H}_4\text{PMo}_6$, 13.0(13.2); $\text{NaNH}_4\text{-C}_6\text{H}_5\text{PMo}_6$, 12.2(12.2); $\text{NaNH}_4\text{-FC}_6\text{H}_4\text{PMo}_6$, 11.3(9.1); $\text{NaNH}_4\text{-F}_3\text{COC}_6\text{H}_4\text{PMo}_6$, 8.3(9.4); **Na-Mo₇**, 10.2(11.2). The first weight loss step for all the TGAs was determined by analyzing the exact cut off point from the 1st derivative graph as depicted in Figure S9-S17. The dissimilarity in the number of crystal waters determined by TGA from that evidenced by elemental analysis could be attributed to the variation in drying periods and aging of the samples at room temperature prior to the measurements. This stage was followed by a second weight loss step involving the release of NH_3 molecules, dimethylarsinate, and organic moieties, culminating in complete structural decomposition. The total weight losses for $\text{NaNH}_4\text{-PMo}_6$, **Na-HPMo₆**, $\text{NaNH}_4\text{-CH}_3\text{PMo}_6$, $\text{NaNH}_4\text{-HO}_2\text{CCH}_2\text{PMo}_6$, $\text{NaNH}_4\text{-HO}_2\text{CC}_2\text{H}_4\text{PMo}_6$, $\text{NaNH}_4\text{-C}_6\text{H}_5\text{PMo}_6$, $\text{NaNH}_4\text{-FC}_6\text{H}_4\text{PMo}_6$, $\text{NaNH}_4\text{-F}_3\text{COC}_6\text{H}_4\text{PMo}_6$, and **Na-Mo₇** at 520 °C were 33.5%, 35.7%, 39%, 37.5%, 39.7%, 37.9%, 41.3%, 40.7%, and 42.5%, respectively.

References

1. APEX Suite of Crystallographic Software, APEX 3, Version 5-2; Bruker AXS Inc.: Madison, WI, 2015.
2. SAINT, Version 7.56a and SADABS Version 2008/1; Bruker AXS Inc.: Madison, WI, 2008.
3. G. M. Sheldrick, A short history of SHELX, *Acta Crystallogr., Sect. A: Found. Crystallogr.* 2008, **A64**, 112-122.
4. G. M. Sheldrick, SHELXL-2014, Program for Crystal Structure Refinement, University of Gottingen: Gottingen, Germany, 2014.
5. CrysAlis^{Pro} Software System, Version 1.171.38.41, Rigaku Oxford Diffraction 2022.
6. ABSPACK, SCALE “Empirical Absorption Correction” CrysAlis Pro–Software Package, Rigaku Oxford Diffraction 2022.
7. I. D. Brown and D. Altermatt, Bond-Valence Parameters Obtained from a Systematic Analysis of the Inorganic Crystal Structure Database, *Acta Crystallogr.* 1985, **B41**, 244-247.

Table S1. Crystal data and structure refinement for **NaNH₄-PMo₆**, **Na-HPMo₆**, **NaNH₄-CH₃PMo₆**, **NaNH₄-HO₂CCH₂PMo₆**, **Na-HO₂CC₂H₄PMo₆.dmsO**, **NaNH₄-C₆H₅PMo₆**, **NaNH₄-FC₆H₄PMo₆**, **NaNH₄-F₃COC₆H₄PMo₆**, and **Na-Mo₇**.

compound	NaNH ₄ -PMo ₆	Na-HPMo ₆	NaNH ₄ -CH ₃ PMo ₆	NaNH ₄ -HO ₂ CCH ₂ PMo ₆	Na-HO ₂ CC ₂ H ₄ PMo ₆ .dmsO	NaNH ₄ -C ₆ H ₅ PMo ₆	NaNH ₄ -FC ₆ H ₄ PMo ₆	NaNH ₄ -F ₃ COC ₆ H ₄ PMo ₆	Na-Mo ₇
empirical formula ^a	C ₆ H ₃₈ As ₃ Mo ₆ NNa _{1.8} O ₃₁ PCl _{0.8}	C ₆ H _{44.8} O ₃₅ Na _{1.2} PAs ₃ Mo ₆	C ₇ H ₅₀ NO ₃₅ NaPAs ₃ Mo ₆	C ₈ H _{45.6} N _{0.9} O ₃₅ Na _{1.6} PAs ₃ Mo ₆ Cl _{0.5}	C ₂₇ H ₈₂ O ₃₆ Na ₂ PS ₉ As ₃ Mo ₆	C ₁₂ H _{49.2} N _{1.3} O ₃₃ Na _{0.7} PAs ₃ Mo ₆	C ₁₂ H ₄₅ NO ₃₂ FNaPAs ₃ Mo ₆	C _{13.6} H _{50.8} N _{1.5} O _{34.6} F ₃ Na _{0.8} PAs _{3.3} Mo ₆	C ₈ H ₅₄ As ₄ Mo ₇ NNaO ₃₈
fw, ^a g mol ⁻¹	1521.48	1536.17	1562.84	1600.53	2148.81	1587.39	1588.85	1718.39	1766.77
cryst syst	Trigonal	trigonal	trigonal	trigonal	monoclinic	trigonal	trigonal	trigonal	trigonal
space group	R-3	R-3	R-3	R-3	P2 ₁ /c	R-3	R-3	R-3	R-3
a, Å	19.6625(6)	19.5011(3)	19.4432(3)	19.6852(3)	15.51260(10)	19.6927(3)	19.7297(3)	19.6877(2)	19.5197(6)
b, Å	19.6625(6)	19.5011(3)	19.4432(3)	19.6852(3)	13.09310(10)	19.6927(3)	19.7297(3)	19.6877(2)	19.5197(6)
c, Å	18.9655(8)	19.1833(3)	19.1654(3)	18.9794(3)	35.1451(3)	19.3398(3)	19.3919(4)	19.6146(2)	19.2066(8)
α, deg	90	90	90	90	90	90	90	90	90
β, deg	90	90	90	90	102.5610(10)	90	90	90	90
γ, deg	120	120	120	120	90	120	120	120	120
volume, Å ³	6350.0(5)	6317.9(2)	6274.6(2)	6369.3(2)	6967.40(10)	6495.2(2)	6537.2(2)	6584.15(15)	6337.6(5)
Z	6	6	6	6	4	6	6	6	6
D _{calc} , g cm ⁻³	2.387	2.423	2.482	2.504	2.049	2.435	2.422	2.600	2.777
abs coeff, mm ⁻¹	4.246	4.221	4.251	4.227	2.849	4.103	4.081	4.294	5.243
F(000)	4370.0	4440.0	4536.0	4632.0	4256.0	4608.0	4596.0	4988.0	5100.0
2θ range for data collection, deg	7.178 - 54.204	4.884 - 61.878	4.89 - 61.948	4.912 - 68.19	4.73 - 62.286	4.842-68.038	4.83 - 59.556	4.792 - 59.626	7.232 - 56.56
completeness to	99.7	88.8	87.3	93.2	92.2	93.7	89.1	92.8	99.8

$\Theta_{\max}, \%$									
index ranges	$-25 \leq h \leq 25,$ $-25 \leq k \leq 25,$ $-24 \leq l \leq 24$	$-27 \leq h \leq 26,$ $26 \leq k \leq 26,$ $-25 \leq l \leq 27$	$-27 \leq h \leq 26,$ $-27 \leq k \leq 25,$ $-24 \leq l \leq 26$	$-30 \leq h \leq 30,$ $-30 \leq k \leq 31,$ $-28 \leq l \leq 28$	$-21 \leq h \leq 22,$ $-18 \leq k \leq 18,$ $-45 \leq l \leq 47$	$-29 \leq h \leq 30,$ $30 \leq k \leq 30,$ $-29 \leq l \leq 29$	$-26 \leq h \leq 27,$ $25 \leq k \leq 26,$ $-25 \leq l \leq 27$	$-26 \leq h \leq 27,$ $-27 \leq k \leq 26,$ $-27 \leq l \leq 26$	$-26 \leq h \leq 25,$ $26 \leq k \leq 26,$ $25 \leq l \leq 25$
reflns collected	28014	31796	31581	70017	463526	72890	36414	88743	44814
indep reflns	3112	3973	3881	5431	20745	5534	3705	3898	3497
R(int)	0.0842	0.0387	0.0282	0.0514	0.0597	0.0524	0.0371	0.0282	0.1181
data/restraints/par am	3112/0/146	3973/0/162	3881/0/166	5431/0/160	20745/0/438	5534/0/164	3705/0/172	3898/0/159	3497/0/162
GOF on F^2	1.000	1.006	1.004	1.000	1.011	1.000	1.007	1.004	1.001
$R_1, {}^b wR_2^c$ [$I > 2\sigma(I)$]	$R_1 = 0.0449,$ $wR_2 = 0.1149$	$R_1 = 0.0274,$ $wR_2 = 0.0842$	$R_1 = 0.0244,$ $wR_2 = 0.0705$	$R_1 = 0.0411,$ $wR_2 = 0.1220$	$R_1 = 0.0673,$ $wR_2 = 0.1754$	$R_1 = 0.0364,$ $wR_2 = 0.1108$	$R_1 = 0.0333,$ $wR_2 = 0.0936$	$R_1 = 0.0359,$ $wR_2 = 0.1065$	$R_1 = 0.0528,$ $wR_2 = 0.1455$
$R_1, {}^b wR_2^c$ (all data)	$R_1 = 0.0619,$ $wR_2 = 0.1254$	$R_1 = 0.0316,$ $wR_2 = 0.0866$	$R_1 = 0.0280,$ $wR_2 = 0.0721$	$R_1 = 0.0558,$ $wR_2 = 0.1307$	$R_1 = 0.0752,$ $wR_2 = 0.1800$	$R_1 = 0.0464,$ $wR_2 = 0.1205$	$R_1 = 0.0418,$ $wR_2 = 0.1042$	$R_1 = 0.0411,$ $wR_2 = 0.1153$	$R_1 = 0.0714,$ $wR_2 = 0.1601$
largest diff peak and hole, $e \text{ \AA}^{-3}$	1.281 and -1.032	2.139 and -0.877	1.986 and -0.722	4.67 and -1.44	3.41 and -2.52	3.51 and -1.14	1.92 and -0.98	1.76 and -1.63	2.23 and -6.02

^[a] The entries represent the actual formula units and weights obtained from bulk elemental analysis, except for **Na-HO₂CC₂H₄PMo₆·dmsO**, where the formula is reported based on single-crystal XRD data. ^b $R_1 = \Sigma||F_o| - |F_c||/\Sigma|F_o|$. ^c $wR_2 = [\Sigma w(F_o^2 - F_c^2)^2/\Sigma w(F_o^2)^2]^{1/2}$.

Table S2. Bond valence sum (BVS) values for **NaNH₄-PMo₆**. Bond Valence (v_{ij}) = $\exp[(R_{ij}-d_{ij})/b]$ (R_{ij} = bond valence parameter; $b = 0.37$); Bond Valence Sum (V_i) = $\sum_j v_{ij}$.

i	j	d_{ij} (Å)	v_{ij}	i	j	d_{ij} (Å)	v_{ij}
Mo1	O1T	1.69	1.797661	Mo2	O2T	1.682	1.836953
	O21	1.942	0.909742		O12	1.939	0.917148
	O12	1.937	0.922119		O21	1.949	0.892692
	O1AS	2.099	0.595164		O2AS	2.076	0.633334
	O1A	2.112	0.574616		O1A	2.123	0.557784
	O2P	2.31	0.336489		O2P	2.302	0.343844
			5.13579				5.181755
O1A	Mo1	2.112	0.574616	O1P	P	1.52	1.299737
	Mo2	2.123	0.557784				
			1.1324				

Table S3. Bond valence sum (BVS) values for **Na-HPMo₆**. Bond Valence (v_{ij}) = $\exp[(R_{ij}-d_{ij})/b]$ (R_{ij} = bond valence parameter; $b = 0.37$); Bond Valence Sum (V_i) = $\sum_j v_{ij}$.

i	j	d_{ij} (Å)	v_{ij}	i	j	d_{ij} (Å)	v_{ij}
Mo1	O1A	1.683	1.831995	Mo2	O2A	1.689	1.802526
	O12	1.936	0.924615		O12	1.933	0.932142
	O21	1.952	0.885483		O21	1.945	0.902395
	O2AS	2.07	0.643688		O1AS	2.087	0.614783
	O2B	2.126	0.55328		O2B	2.107	0.582433
	O1P	2.333	0.316209		O1P	2.355	0.297956
			5.15527				5.132235
O2B	Mo2	2.107	0.582433				
	Mo1	2.126	0.55328				
			1.135713				

Table S4. Bond valence sum (BVS) values for **NaNH₄-CH₃PMo₆**. Bond Valence (v_{ij}) = $\exp[(R_{ij}-d_{ij})/b]$ (R_{ij} = bond valence parameter; $b = 0.37$); Bond Valence Sum (V_i) = $\sum_j v_{ij}$.

i	j	d_{ij} (Å)	v_{ij}	i	j	d_{ij} (Å)	v_{ij}
Mo1	O1A	1.692	1.78797	Mo2	O2A	1.685	1.822119
	O12	1.93	0.93973		O12	1.932	0.934665
	O21	1.9443	0.904104		O21	1.9509	0.88812
	O1AS	2.09	0.609818		O2AS	2.069	0.64543
	O2B	2.111	0.576171		O2B	2.125	0.554777
	O1P	2.3343	0.3151		O1P	2.316	0.331077
			5.132894				5.176187
O2B	Mo1	2.111	0.576171				
	Mo2	2.125	0.554777				
			1.130948				

Table S5. Bond valence sum (BVS) values for **NaNH₄-HO₂CCH₂PMo₆**. Bond Valence (v_{ij}) = $\exp[(R_{ij}-d_{ij})/b]$ (R_{ij} = bond valence parameter; $b = 0.37$); Bond Valence Sum (V_i) = $\sum_j v_{ij}$.

i	j	d_{ij} (Å)	v_{ij}	i	j	d_{ij} (Å)	v_{ij}
Mo1	O1A	1.684	1.82705	Mo2	O2A	1.69	1.797661
	O12	1.934	0.929626		O12	1.932	0.934665
	O21	1.948	0.895108		O21	1.943	0.907286
	O1AS	2.071	0.641951		O2AS	2.081	0.624833
	O2B	2.125	0.554777		O2B	2.109	0.579294
	O1P	2.323	0.324872		O1P	2.334	0.315356
			5.173384				5.159095
O2B	Mo2	2.125	0.554777				
	Mo1	2.109	0.579294				
			1.13407				

Table S6. Bond valence sum (BVS) values for **Na-HO₂CC₂H₄PMo₆·dmsO**. Bond Valence (v_{ij}) = $\exp[(R_{ij}-d_{ij})/b]$ (R_{ij} = bond valence parameter; $b = 0.37$); Bond Valence Sum (V_i) = $\sum_j v_{ij}$.

i	j	d_{ij} (Å)	v_{ij}	i	j	d_{ij} (Å)	v_{ij}
Mo1	O1T	1.689	1.802526	Mo2	O2T	1.693	1.783144
	O16	1.936	0.924615		O23	1.935	0.927117
	O61	1.936	0.924615		O32	1.942	0.909742
	O1A1	2.077	0.631625		O2A1	2.076	0.633334
	O12	2.122	0.559293		O12	2.116	0.568437
	O1P	2.323	0.324872		O1P	2.347	0.304468
			5.167546				5.126242
Mo3	O3T	1.687	1.812296	Mo4	O4T	1.691	1.792809
	O23	1.928	0.944824		O45	1.933	0.932142
	O32	1.932	0.934665		O54	1.933	0.932142
	O1A2	2.074	0.636767		O2A2	2.065	0.652446
	O34	2.12	0.562325		O34	2.095	0.601633
	O2P	2.368	0.287669		O2P	2.333	0.316209
			5.178545				5.227381
Mo5	O5T	1.69	1.797661	Mo6	O6T	1.692	1.78797
	O45	1.937	0.922119		O16	1.929	0.942274
	O54	1.94	0.914673		O61	1.929	0.942274
	O1A3	2.068	0.647177		O2A3	2.067	0.648929
	O56	2.106	0.58401		O56	2.113	0.573065
	O3P	2.348	0.303646		O3P	2.397	0.265983
			5.169286				5.160494
O56	Mo5	2.106	0.58401	O12	Mo2	2.116	0.568437
	Mo6	2.113	0.573065		Mo1	2.122	0.559293
			1.157075				1.12773
O34	Mo4	2.095	0.601633	O1	C3	1.336	1.157134
	Mo3	2.12	0.562325				
			1.163958				

Table S7. Bond valence sum (BVS) values for **NaNH₄-C₆H₅PMo₆**. Bond Valence (v_{ij}) = $\exp[(R_{ij}-d_{ij})/b]$ (R_{ij} = bond valence parameter; $b = 0.37$); Bond Valence Sum (V_i) = $\sum_j v_{ij}$.

i	j	d_{ij} (Å)	v_{ij}	i	j	d_{ij} (Å)	v_{ij}
Mo1	O1A	1.686	1.817201	Mo2	O2A	1.687	1.812296
	O12	1.928	0.944824		O12	1.93	0.93973
	O21	1.949	0.892692		O21	1.947	0.897531
	O2AS	2.07	0.643688		O1AS	2.086	0.616446
	O1B	2.127	0.551786		O1B	2.11	0.57773
	O1P	2.322	0.325751		O1P	2.342	0.30861
			5.175943				5.152344
O1B	Mo2	2.11	0.57773				
	Mo1	2.127	0.551786				
			1.129516				

Table S8. Bond valence sum (BVS) values for **NaNH₄-FC₆H₄PMo₆**. Bond Valence (v_{ij}) = $\exp[(R_{ij}-d_{ij})/b]$ (R_{ij} = bond valence parameter; $b = 0.37$); Bond Valence Sum (V_i) = $\sum_j v_{ij}$.

i	j	d_{ij} (Å)	v_{ij}	i	j	d_{ij} (Å)	v_{ij}
Mo1	O1P	2.314	0.332871	Mo2	O2	1.688	1.807405
	O1A	2.126	0.55328		O1A	2.109	0.579294
	O1B	1.683	1.831995		O1P	2.34	0.310283
	O2AS	2.071	0.641951		O21	1.947	0.897531
	O21	1.952	0.885483		O12	1.93	0.93973
	O12	1.934	0.929626		O1AS	2.088	0.613123
			5.175206				5.147366
O1A	Mo2	2.109	0.579294				
	Mo1	2.126	0.55328				
			1.132574				

Table S9. Bond valence sum (BVS) values for **NaNH₄-F₃COC₆H₄PMo₆**. Bond Valence (v_{ij}) = $\exp[(R_{ij}-d_{ij})/b]$ (R_{ij} = bond valence parameter; $b = 0.37$); Bond Valence Sum (V_i) = $\sum_j v_{ij}$.

i	j	d_{ij} (Å)	v_{ij}	i	j	d_{ij} (Å)	v_{ij}
Mo1	O12	1.933	0.932142	Mo2	O2AS	2.071	0.641951
	O2B	2.111	0.576171		O12	1.931	0.937194
	O1AS	2.08	0.626524		O21	1.951	0.88788
	O1	1.687	1.812296		O2B	2.129	0.548812
	O21	1.947	0.897531		O1P	2.312	0.334675
	O1P	2.35	0.302009		O2A	1.685	1.822119
			5.146673				5.172631
O2B	Mo2	2.129	0.548812				
	Mo1	2.111	0.576171				
			1.124983				

Table S10. Bond valence sum (BVS) values for **Na-Mo₇**. Bond Valence (v_{ij}) = $\exp[(R_{ij}-d_{ij})/b]$ (R_{ij} = bond valence parameter; $b = 0.37$); Bond Valence Sum (V_i) = $\sum_j v_{ij}$.

i	j	d_{ij} (Å)	v_{ij}	i	j	d_{ij} (Å)	v_{ij}
Mo1	O1M1	1.691	1.792809	Mo2	O1M2	1.684	1.82705
	O12M	1.941	0.912204		O12M	1.94	0.914673
	O21M	1.945	0.902395		O21M	1.953	0.883093
	O1AS	2.105	0.58559		O2AS	2.082	0.623147
	O2M1	2.119	0.563847		O2M1	2.134	0.541445
	O13M	2.28	0.364909		O13M	2.273	0.371878
			5.121754				5.161286
Mo3	O13M	1.684	1.826063	O2M1	Mo1	2.1196	0.562933
	O1M3	1.815	1.283678		Mo2	2.1334	0.542324
	O13M	1.684	1.826063				1.105257
	O13M	1.684	1.826063				
		6.761867	O1M3	Mo3	1.815	1.283678	

Table S11. ESI mass spectrometry data of the polyoxomolybdates investigated in negative ion mode. *m/z* values always refer to most intense peak of isotope envelope cluster. The molecular formula refers to the best fit for a simulated mass spectrum.

Compound	Monomeric 2- ion <i>m/z</i> and elemental composition	Monomeric – ion <i>m/z</i>	Dimeric 2- ion <i>m/z</i> and elemental composition
HPMo₆	821.32 Not assigned	1331.088 Mo ₆ PA ₃ C ₆ H ₂₂ O ₂₄ Na	1331.587 Mo ₁₂ P ₂ As ₆ C ₁₂ H ₄₄ O ₄₈ Na ₂
CH₃PMo₆	821.39 Not assigned	1345.23 Mo ₆ PA ₃ C ₇ H ₂₄ O ₂₄ Na	1345.73 Mo ₁₂ P ₂ As ₆ C ₁₄ H ₅₀ O ₄₈ Na ₂
C₆H₅PMo₆	692.54 Mo ₆ PA ₃ C ₁₂ H ₂₇ O ₂₄	1406.07 Mo ₆ PA ₃ C ₁₂ H ₂₇ O ₂₄ Na	1406.57 Mo ₁₂ P ₂ As ₆ C ₂₄ H ₅₄ O ₄₈ Na ₃
HO₂CCH₂PMo₆	684.11 Mo ₆ PA ₃ C ₈ H ₂₄ O ₂₆	1392.22 Mo ₆ PA ₃ C ₈ H ₂₄ O ₂₆ Na	1392.72 Mo ₁₂ P ₂ As ₆ C ₁₆ H ₄₈ O ₅₂ Na ₂
HO₂CC₂H₄PMo₆	Not observed	1403.25 Mo ₆ PA ₃ C ₉ H ₂₆ O ₂₆ Na	1402.22 Mo ₁₂ P ₂ As ₆ C ₁₈ H ₅₂ O ₅₂ Na ₂
Mo₇	683.54 Mo ₇ As ₃ C ₆ H ₁₈ O ₂₄	1390.08 Mo ₇ As ₃ C ₆ H ₂₁ O ₂₅	1390.58 Mo ₁₄ As ₆ C ₁₂ H ₄₀ O ₅₀ Na
PMo₆	662.58 Mo ₆ PA ₃ C ₆ H ₂₂ O ₂₅	1348.15 Mo ₆ PA ₃ C ₆ H ₂₂ O ₂₅ Na	1347.65 Mo ₁₂ P ₂ As ₆ C ₁₂ H ₄₄ O ₅₀ Na ₂
4-FC₆H₄PMo₆	702.12 Mo ₆ PA ₃ C ₁₂ H ₂₃ O ₂₆ F	1424.24 Mo ₆ PA ₃ C ₁₂ H ₂₆ O ₂₄ FNa	1424.23 Not assigned
4-F₃COC₆H₄PMo₆	734.62 Mo ₆ PA ₃ C ₁₃ H ₂₆ O ₂₅ F ₃	1490.23 Mo ₆ PA ₃ C ₁₃ H ₂₆ O ₂₅ F ₃ Na	1490.73 Not assigned

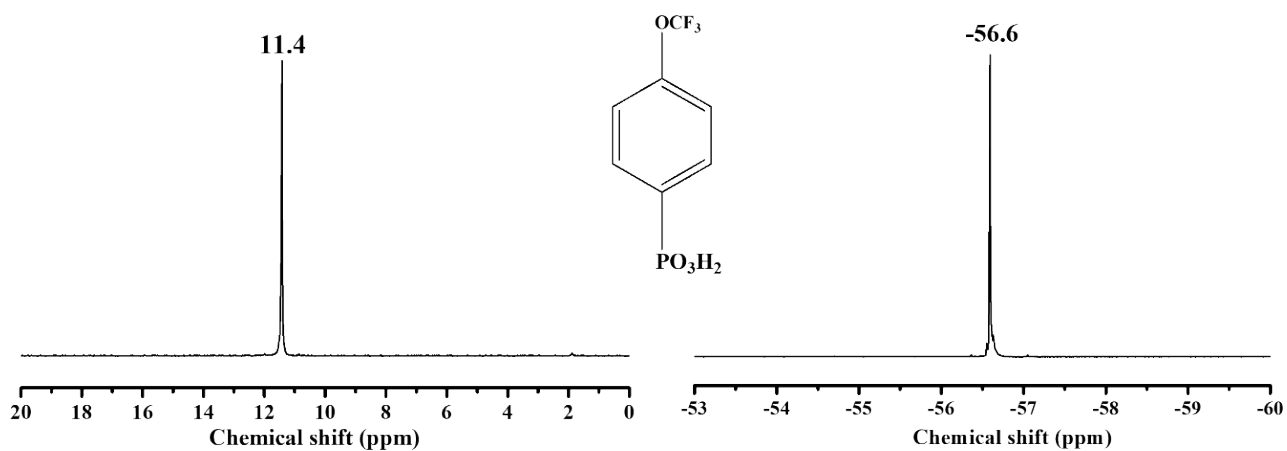


Figure S1. $^{31}P\{^1H\}$ (left) and ^{19}F (right) NMR spectra (4- trifluoromethoxyphenyl) phosphonic acid (L_{POCF_3}), recorded at room temperature in H_2O/D_2O .

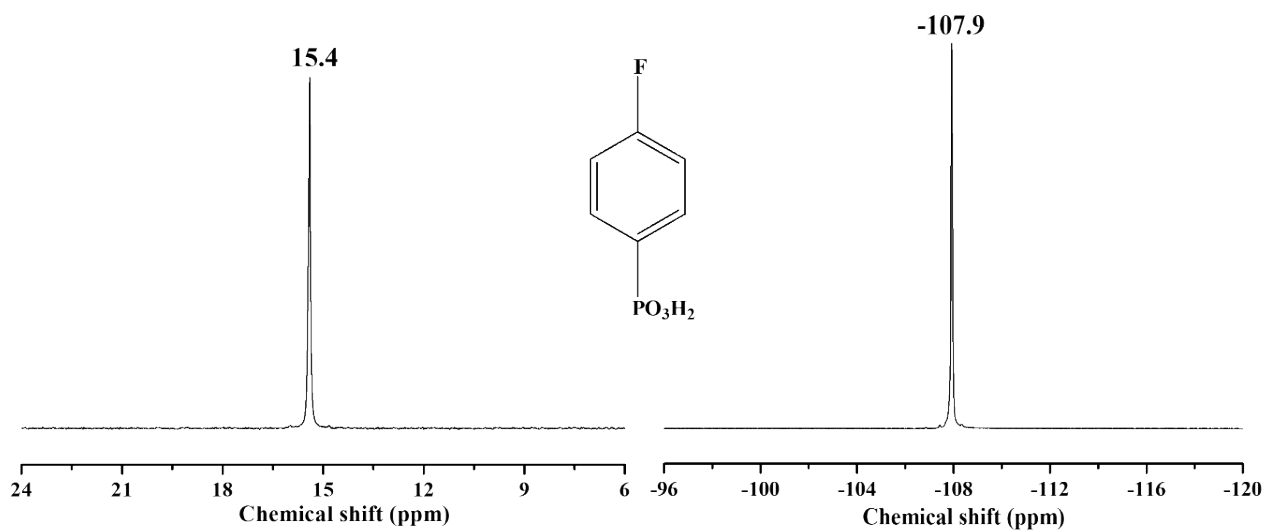


Figure S2. $^{31}P\{^1H\}$ (left) and ^{19}F (right) NMR spectra (4-fluorophenyl) phosphonic acid (L_{PF}), recorded at room temperature in H_2O/D_2O .

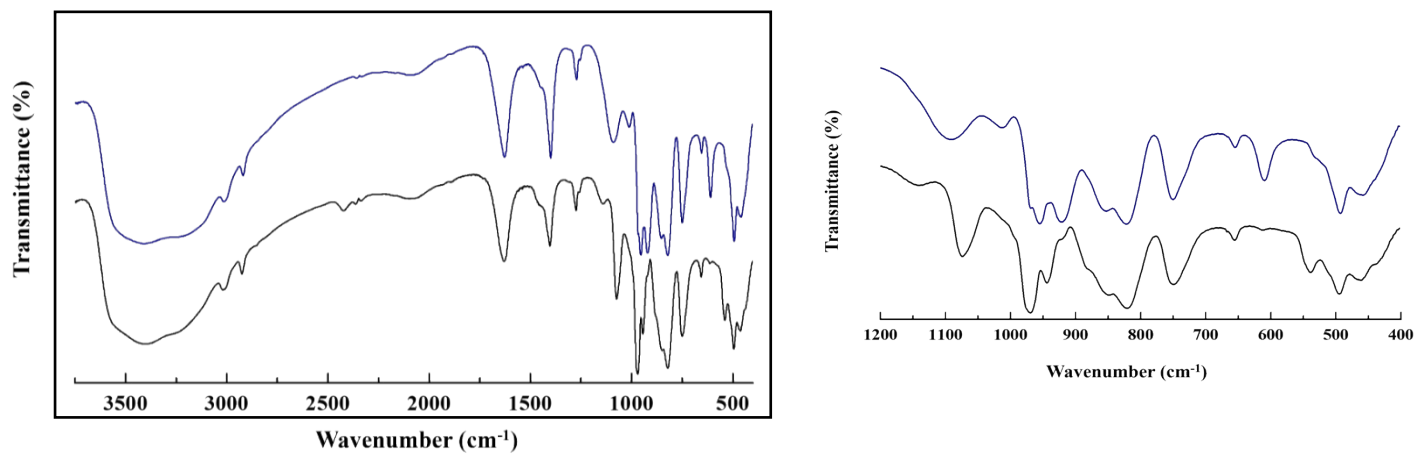


Figure S3. FT-IR spectra of Na-HPMo_6 (black) and $\text{NaNH}_4\text{-PMo}_6$ (blue) on a KBr pellet.

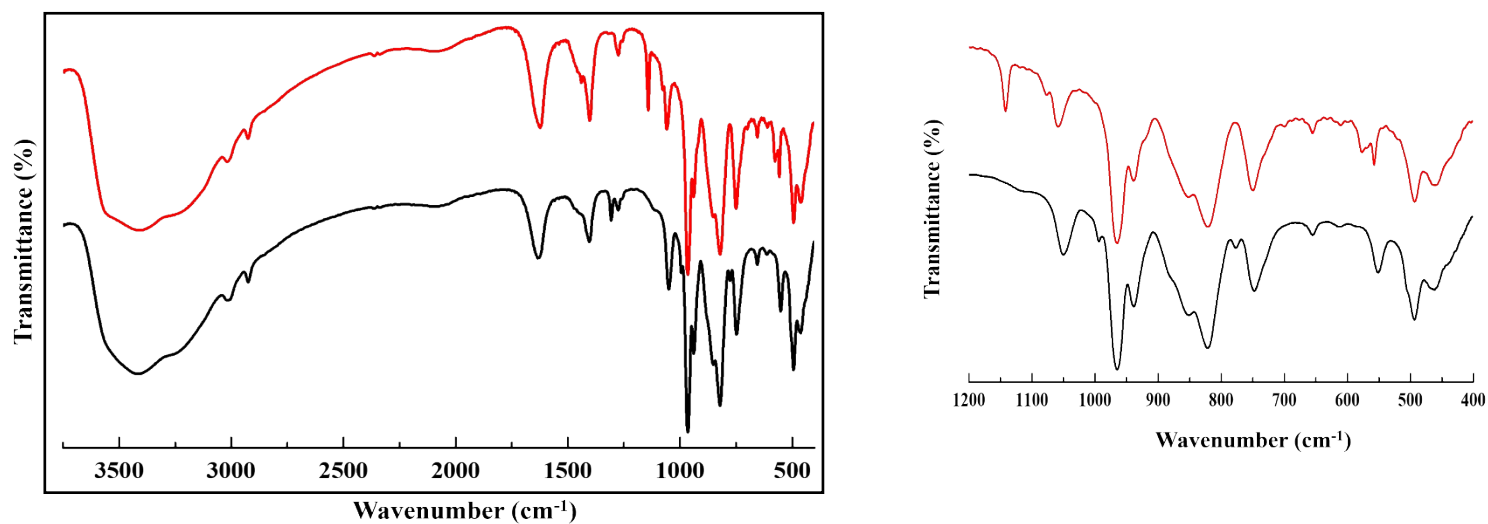


Figure S4. FT-IR spectra of $\text{NaNH}_4\text{-CH}_3\text{PMo}_6$ (black) and $\text{NaNH}_4\text{-C}_6\text{H}_5\text{PMo}_6$ (red) on a KBr pellet.

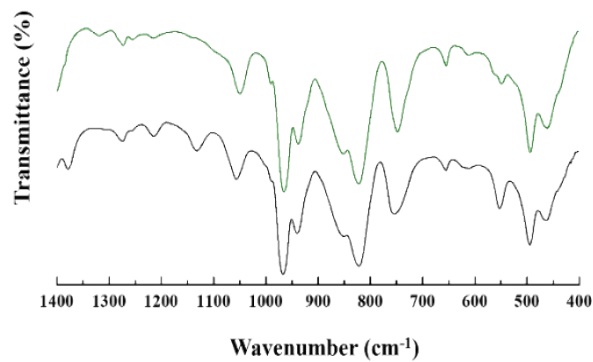
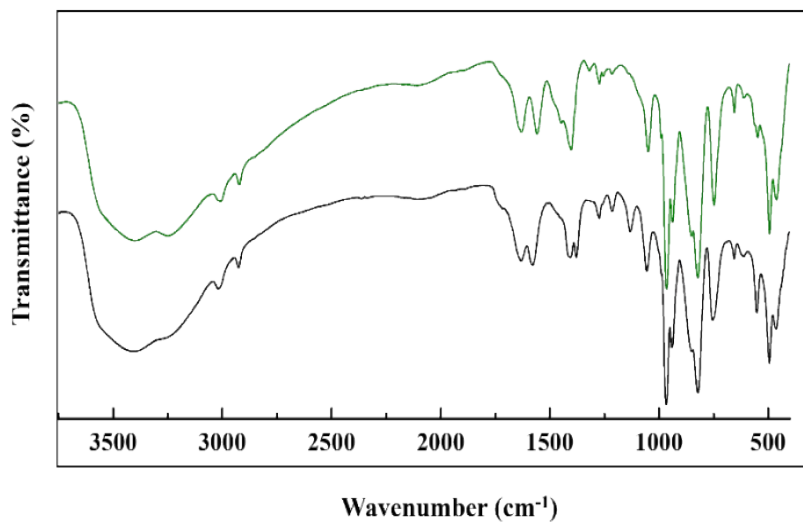


Figure S5. FT-IR spectra of NaNH₄-HO₂CCH₂PMo₆ (black) and NaNH₄-HO₂CC₂H₄PMo₆ (green) on a KBr pellet.

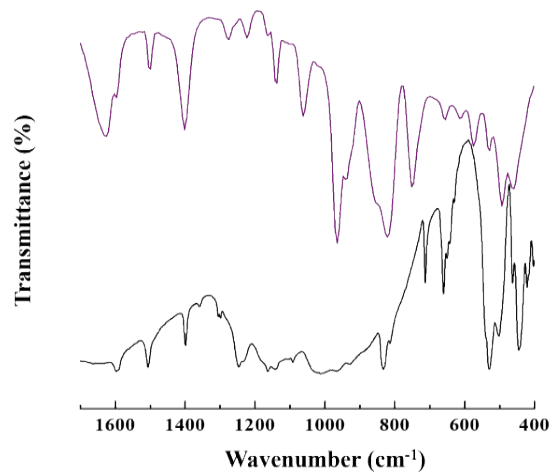
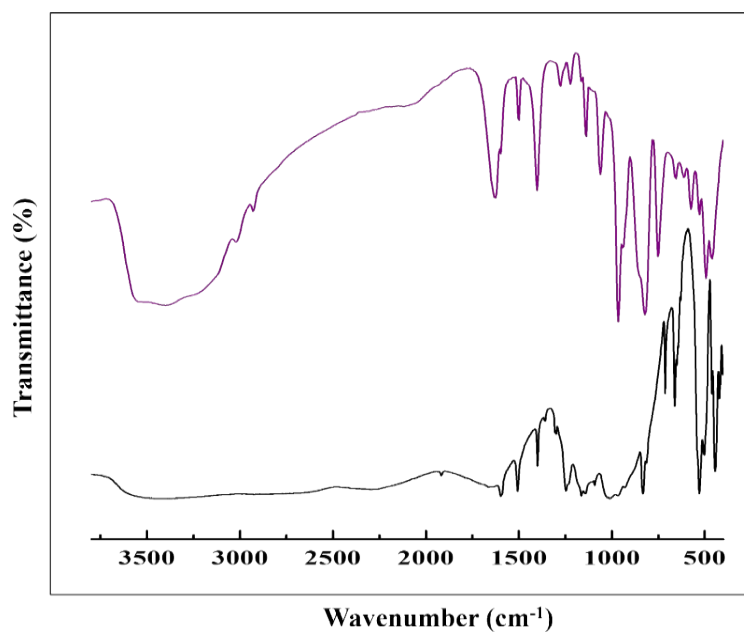


Figure S6. FT-IR spectra of L_pF (black) and NaNH₄-FC₆H₄PMo₆ (violet) on a KBr pellet.

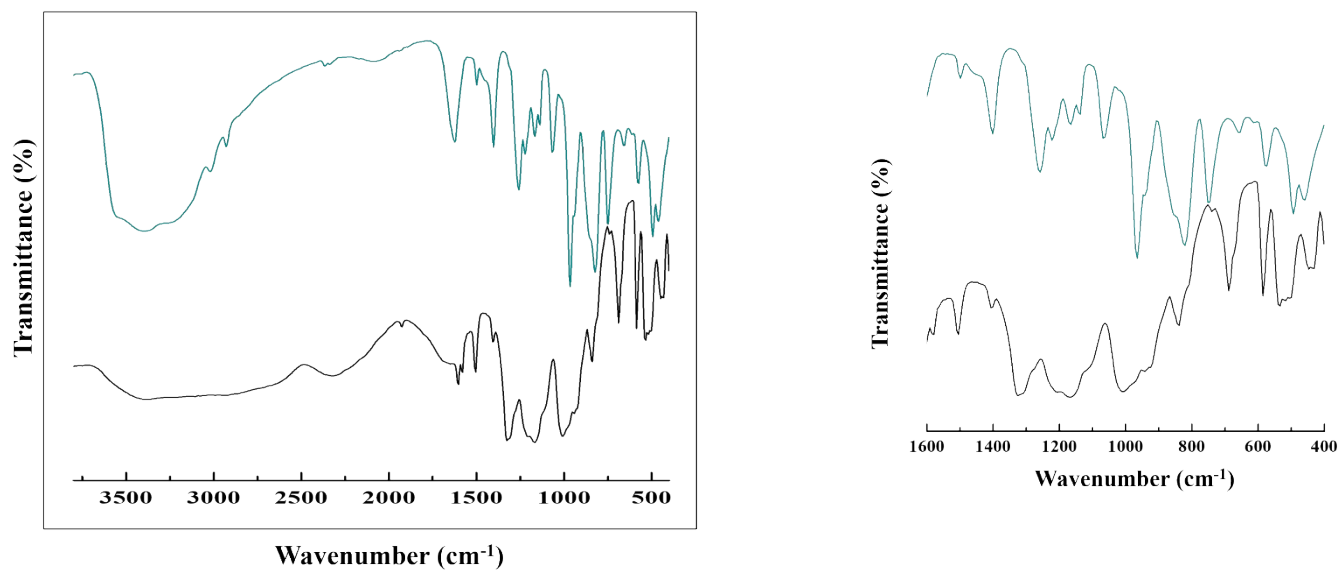


Figure S7. FT-IR spectra of $LPOCF_3$ (black) and $NaNH_4-F_3COC_6H_4PMo_6$ (cyan) on a KBr pellet.

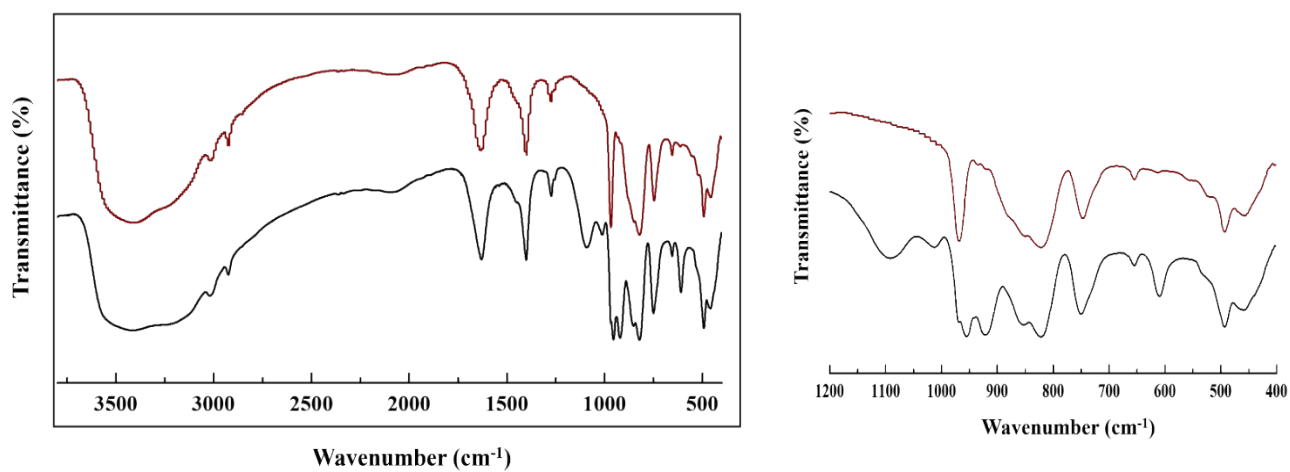


Figure S8. FT-IR spectra of $NaNH_4-PMo_6$ (black) and $Na-Mo_7$ (brown) on a KBr pellet.

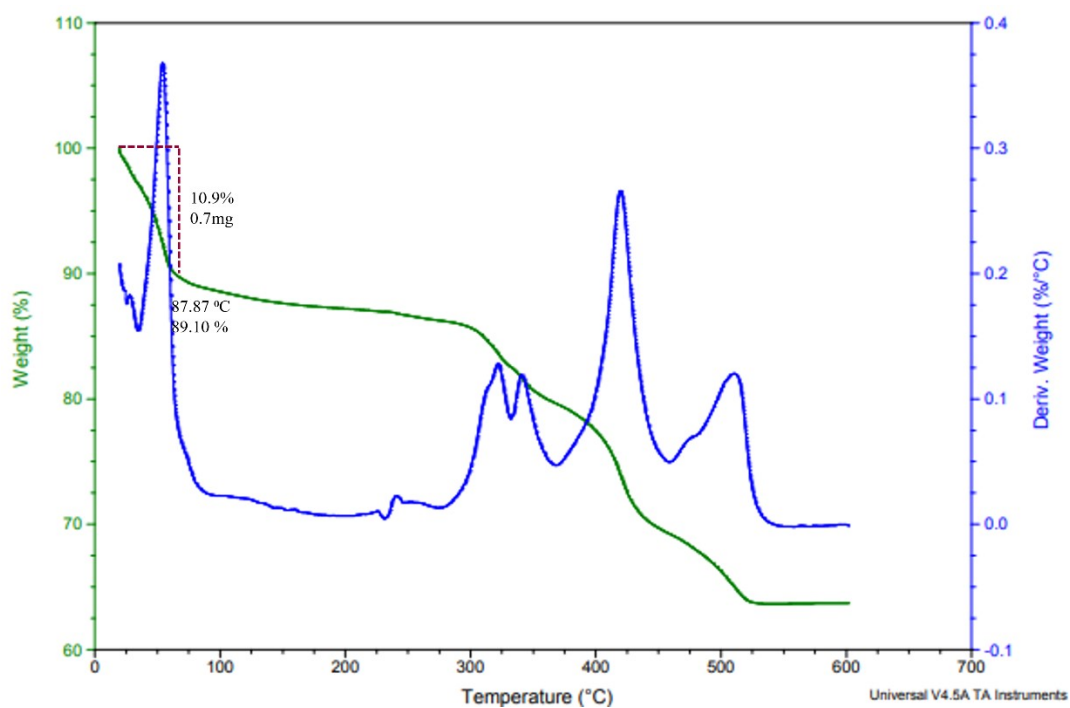


Figure S9. Thermogram of Na-HPMo₆ from room temperature to 600 °C under N₂ atmosphere.

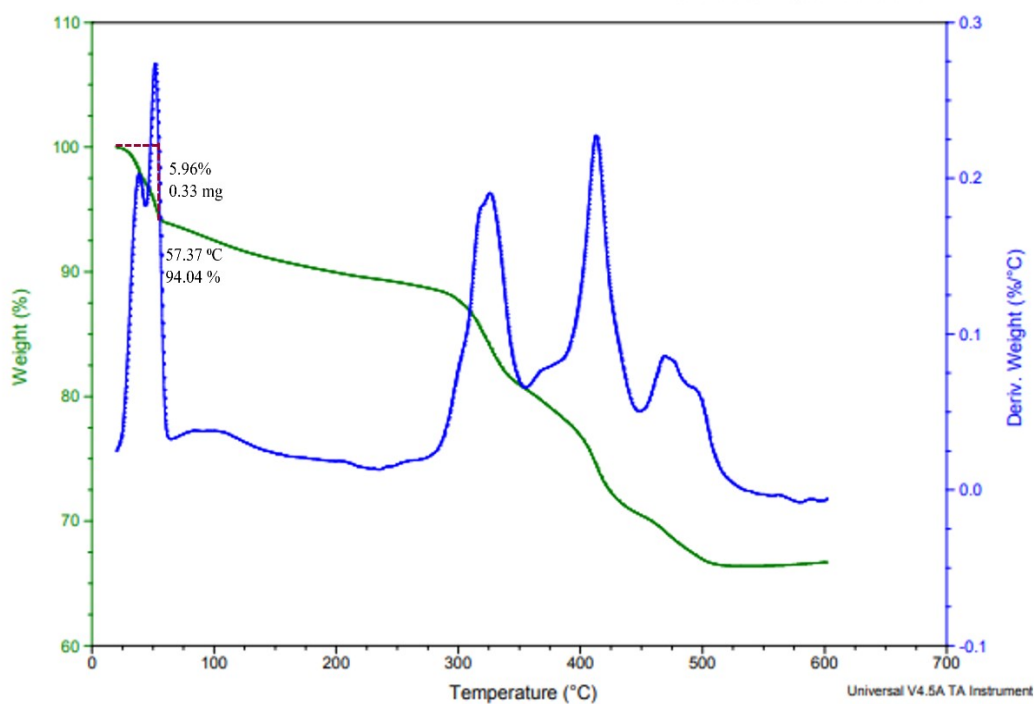


Figure S10. Thermogram of NaNH₄-PMo₆ from room temperature to 600 °C under N₂ atmosphere.

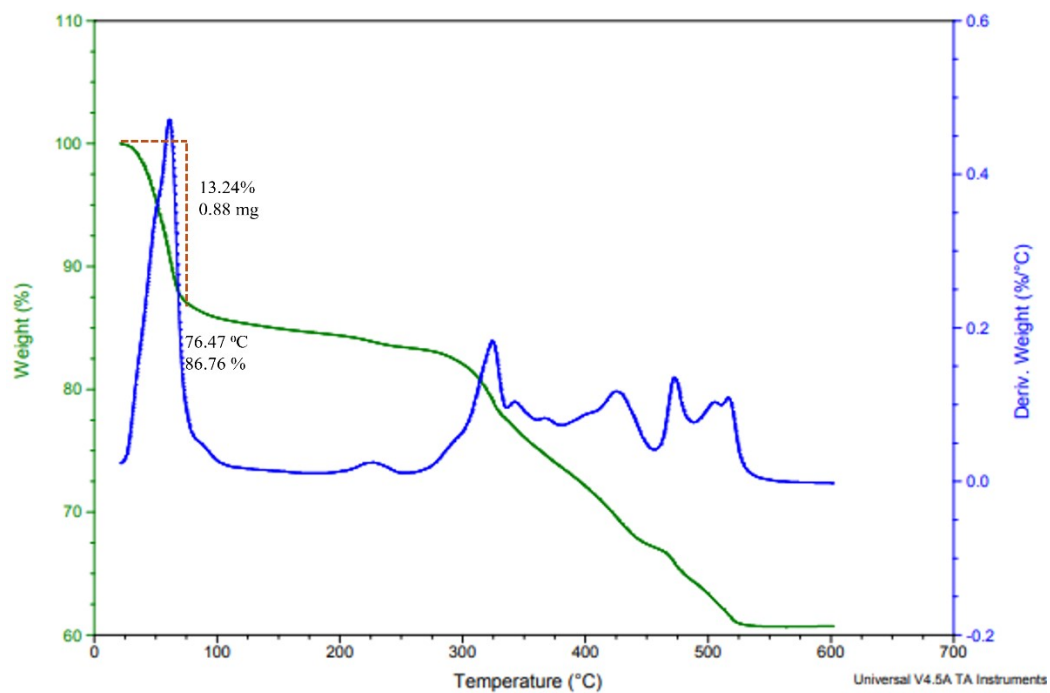


Figure S11. Thermogram of $\text{NaNH}_4\text{-CH}_3\text{PMo}_6$ from room temperature to 600 °C under N_2 atmosphere.

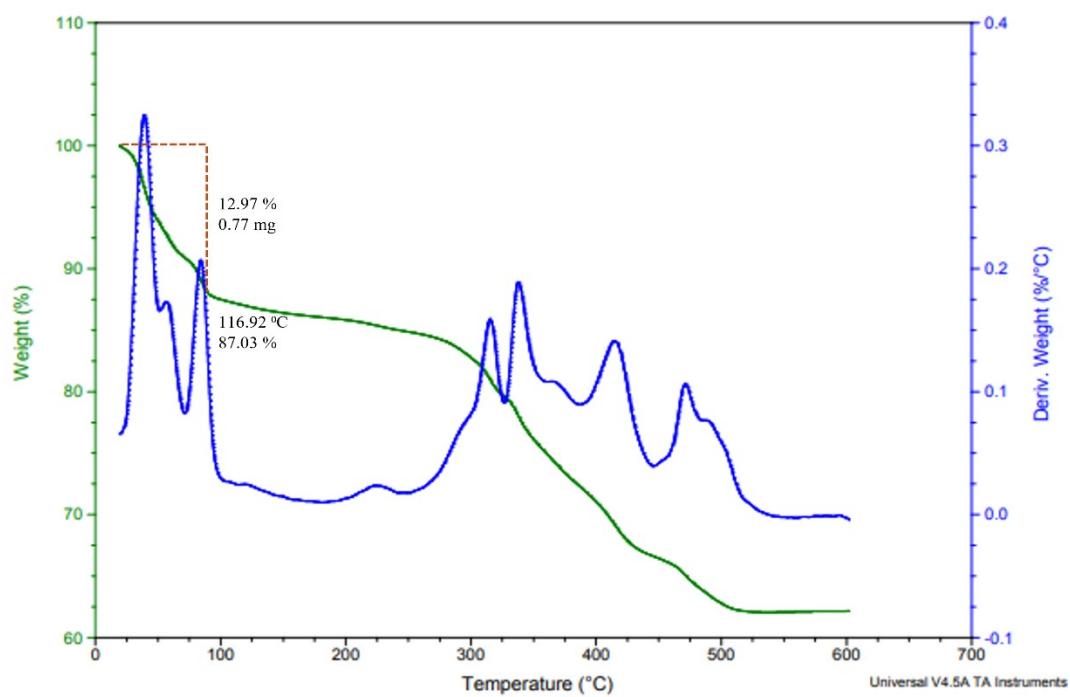


Figure S12. Thermogram of $\text{NaNH}_4\text{-HO}_2\text{CCH}_2\text{PMo}_6$ from room temperature to 600 °C under N_2 atmosphere.

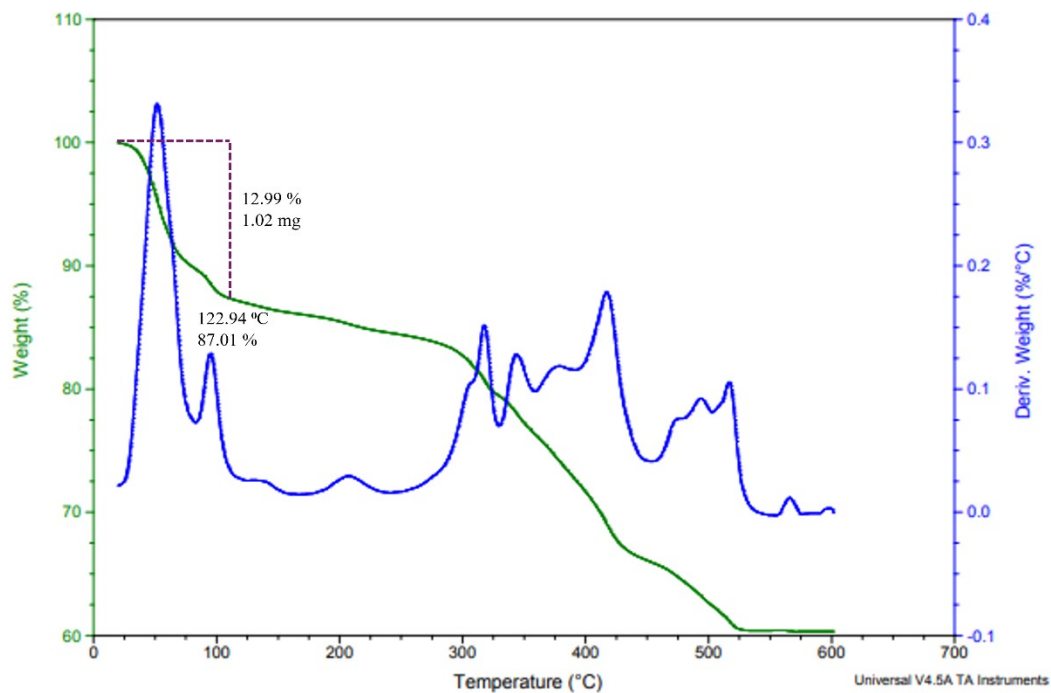


Figure S13. Thermogram of $\text{NaNH}_4\text{-HO}_2\text{CC}_2\text{H}_4\text{PMo}_6$ from room temperature to 600 °C under N_2 atmosphere.

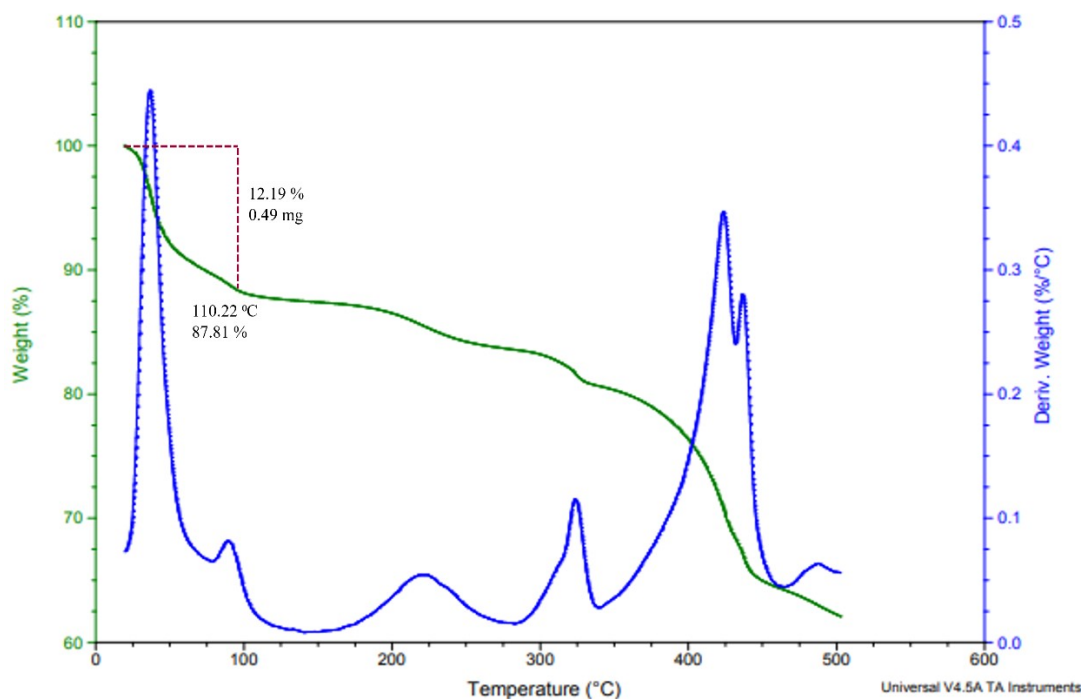


Figure S14. Thermogram of $\text{NaNH}_4\text{-C}_6\text{H}_5\text{PMo}_6$ from room temperature to 500 °C under N_2 atmosphere.

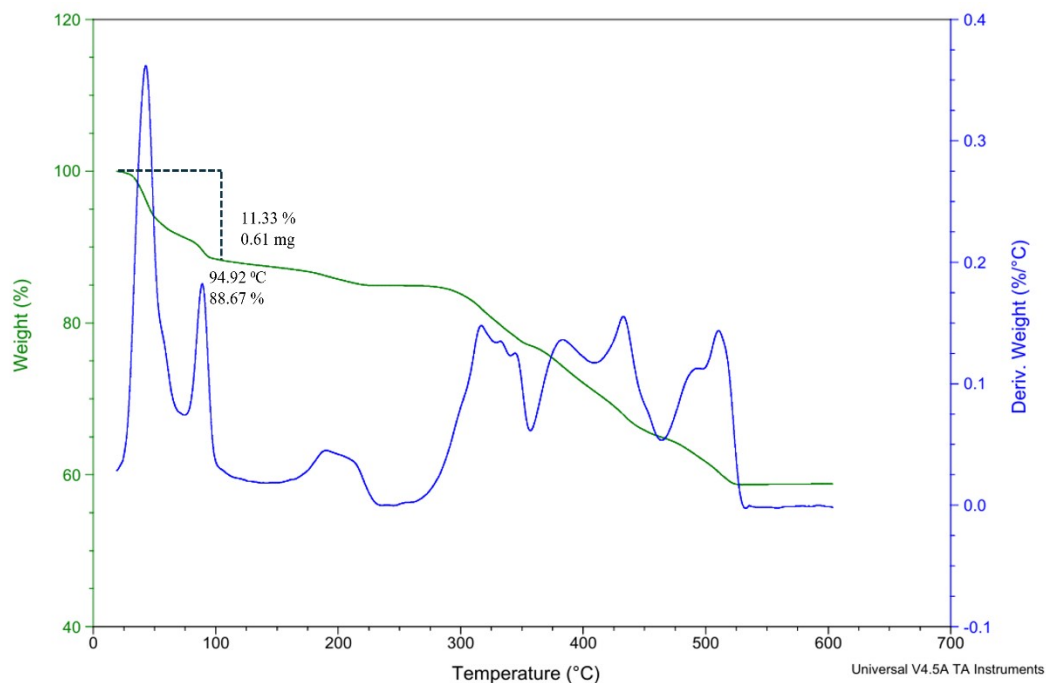


Figure S15. Thermogram of $\text{NaNH}_4\text{-FC}_6\text{H}_4\text{PMo}_6$ from room temperature to 600 °C under N_2 atmosphere.

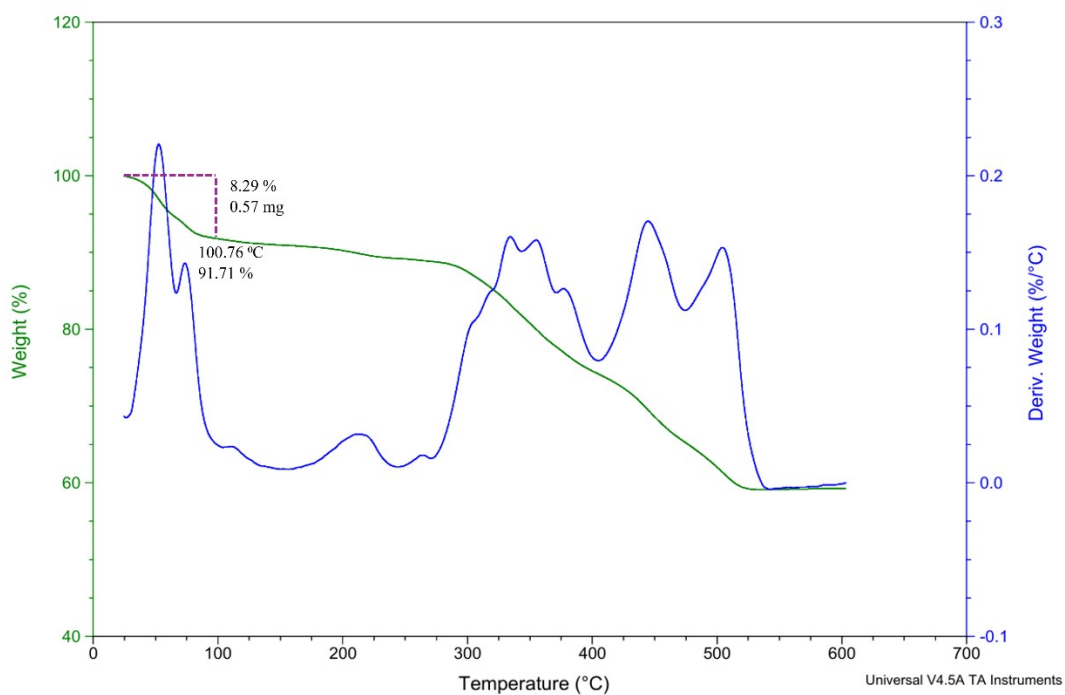


Figure S16. Thermogram of $\text{NaNH}_4\text{-F}_3\text{COC}_6\text{H}_4\text{PMo}_6$ from room temperature to 600 °C under N_2 atmosphere.

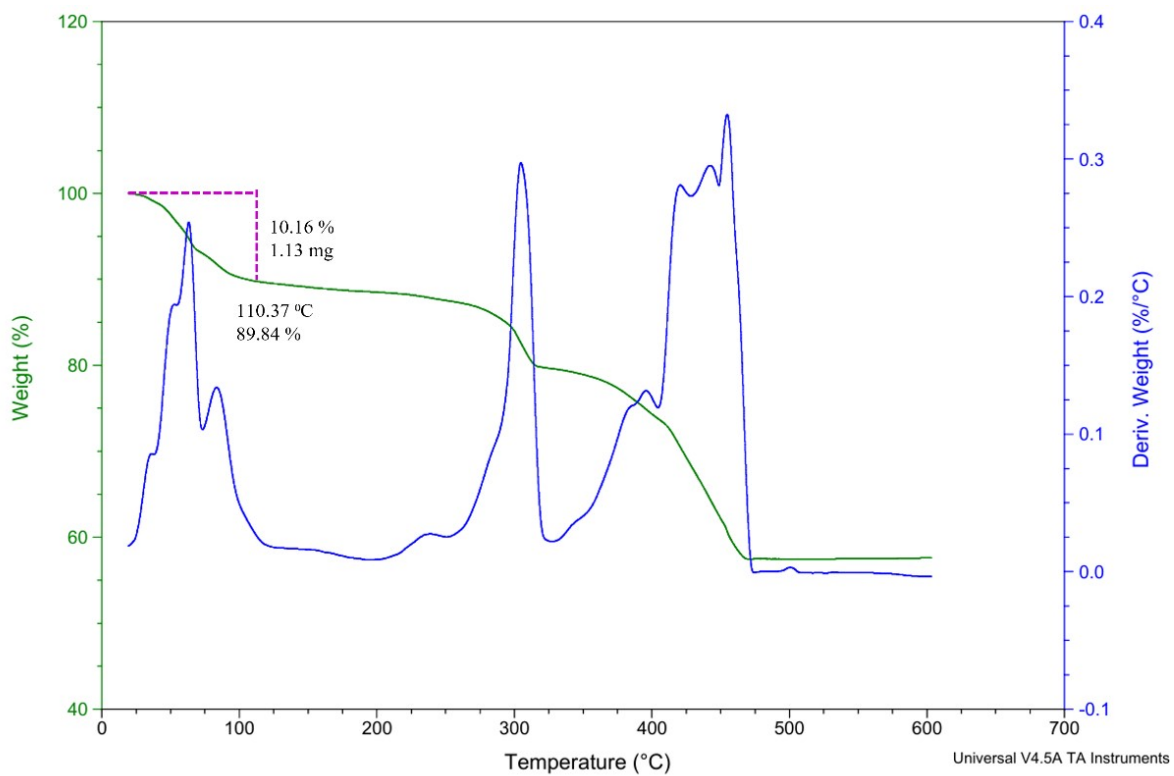


Figure S17. Thermogram of **Na-Mo₇** from room temperature to 600 °C under N₂ atmosphere.

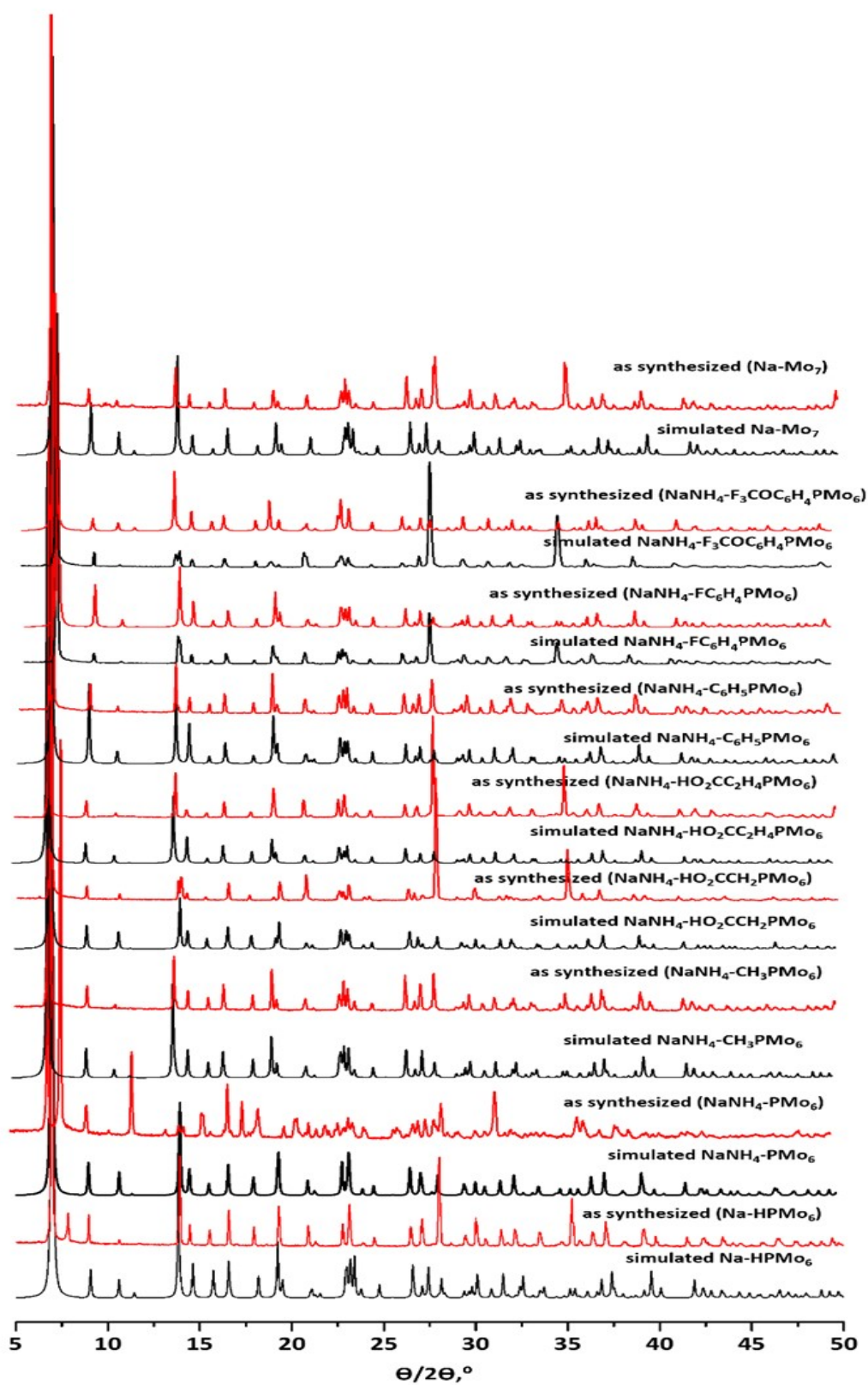


Figure S18. Experimental (red) and simulated (black) PXRD patterns (simulated diffraction patterns derived from single-crystal diffraction data).

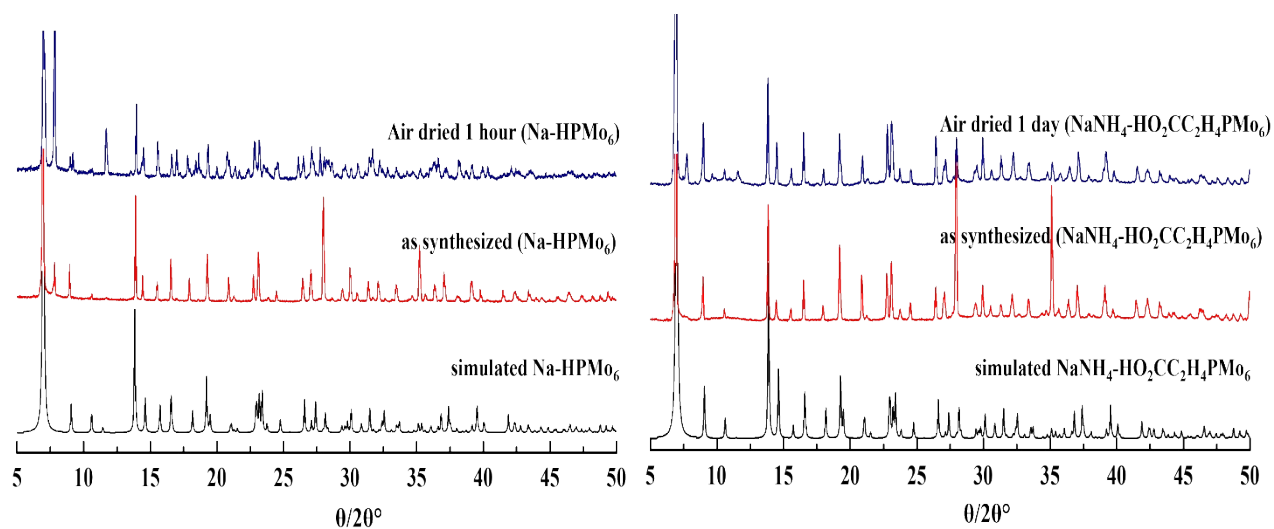


Figure S19. PXRD patterns at various intervals for **Na-HPMo₆** (left) and **NaNH₄-HO₂CC₂H₄PMo₆** (right).

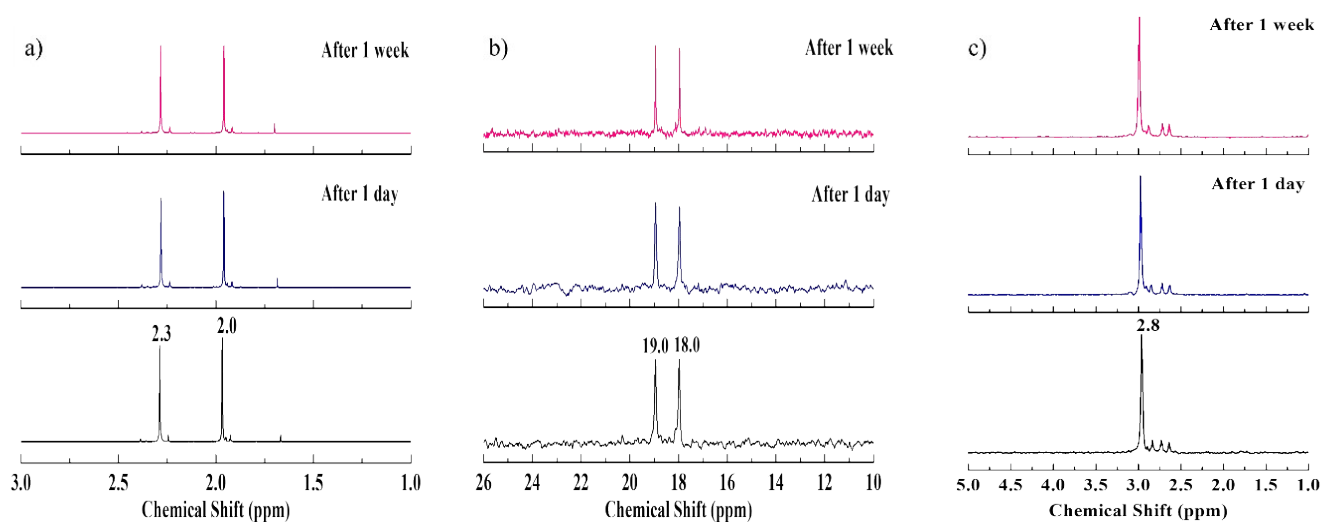


Figure S20. Time dependent (a) ^1H and (b) $^{13}\text{C}\{^1\text{H}\}$ and (c) $^{31}\text{P}\{^1\text{H}\}$ NMR spectra of **NaNH₄-PMo₆** dissolved in $\text{H}_2\text{O}/\text{D}_2\text{O}$ at room temperature.

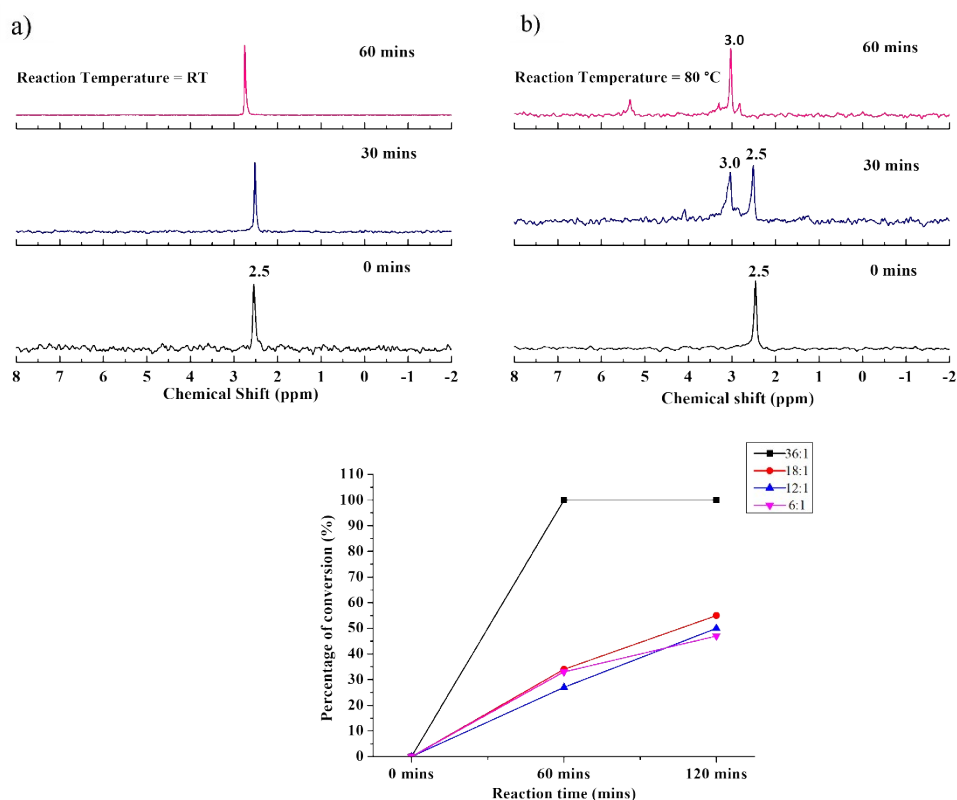


Figure S21. (upper) Monitoring reaction progress by $^{31}\text{P}\{^1\text{H}\}$ NMR of a reaction mixture for PMo_6 with Mo:P ratio of 36:1 over a period of 1 hour at (a) room temperature and (b) 80 °C. (lower) Line graph depicting the formation of PMo_6 in fresh synthesis solution at 80 °C for different ratios of Mo:P as based on $^{31}\text{P}\{^1\text{H}\}$ NMR.

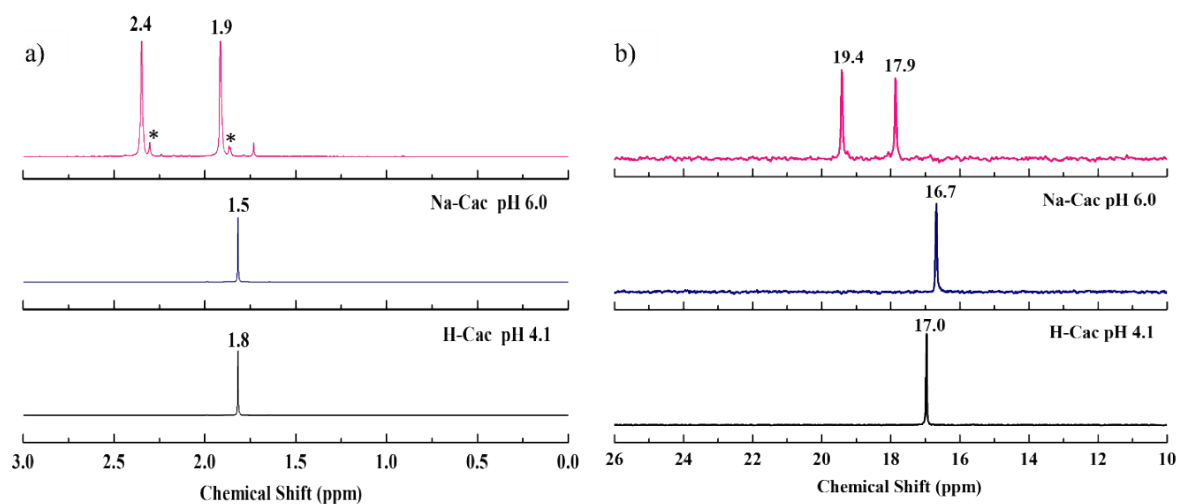


Figure S22. (a) ^1H and (b) $^{13}\text{C}\{^1\text{H}\}$ NMR spectra of Na-HPMo_6 (pink) dissolved in $\text{H}_2\text{O}/\text{D}_2\text{O}$ at room temperature. Sodium cacodylate buffer at pH 6 is used as reference, as the pH of the polyanion salt dissolved in water is also 6.

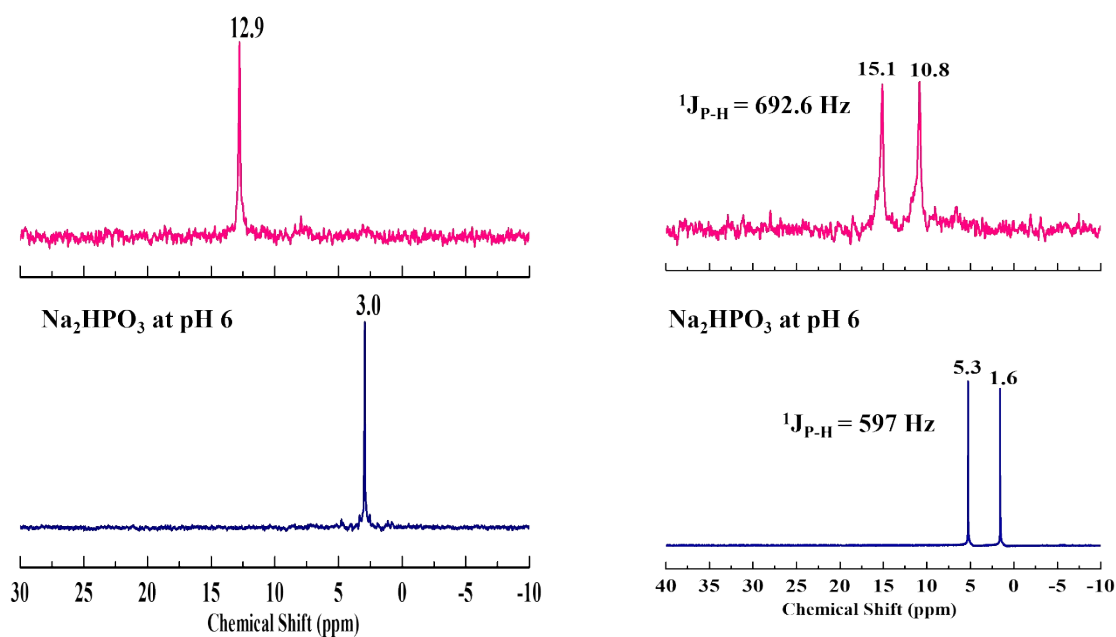


Figure S23. $^{31}\text{P}\{^1\text{H}\}$ (left) and ^{31}P (right) NMR spectra of **Na-HPMo₆** (pink) and the neat hetero group **Na₂HPO₃** (blue) as reference dissolved in $\text{H}_2\text{O}/\text{D}_2\text{O}$ at room temperature.

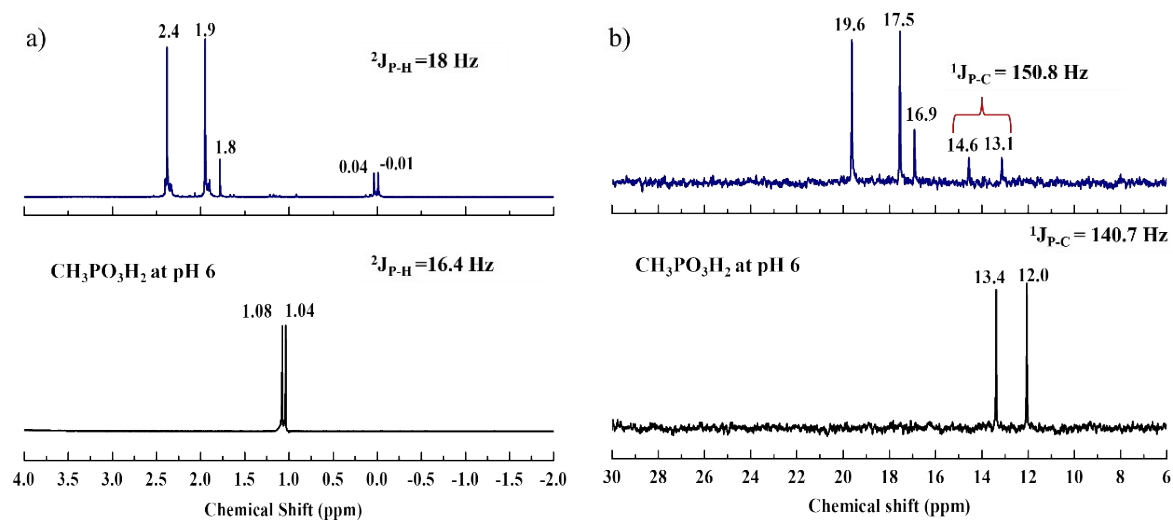


Figure S24. (a) ^1H and (b) $^{13}\text{C}\{^1\text{H}\}$ NMR spectra of $\text{NaNH}_4\text{-CH}_3\text{PMo}_6$ (blue) and the neat hetero group $\text{CH}_3\text{PO}_3\text{H}_2$ (black) as reference, dissolved in $\text{H}_2\text{O}/\text{D}_2\text{O}$ at room temperature.

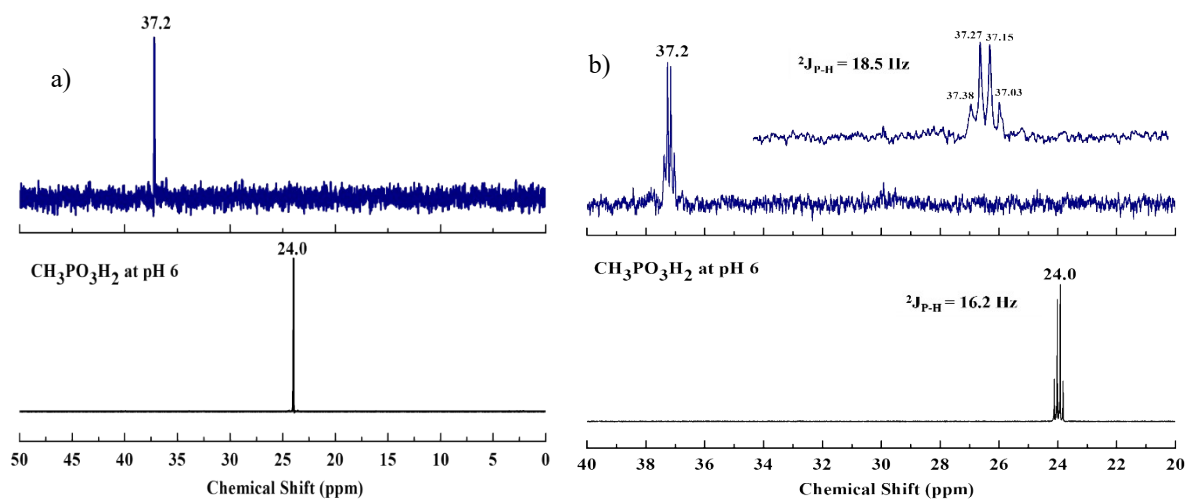


Figure S25. $^{31}\text{P}\{^1\text{H}\}$ (left) and ^{31}P (right) NMR spectra of $\text{NaNH}_4\text{-CH}_3\text{PMo}_6$ (blue) and the neat hetero group $\text{CH}_3\text{PO}_3\text{H}_2$ (black) as reference, dissolved in $\text{H}_2\text{O}/\text{D}_2\text{O}$ at room temperature.

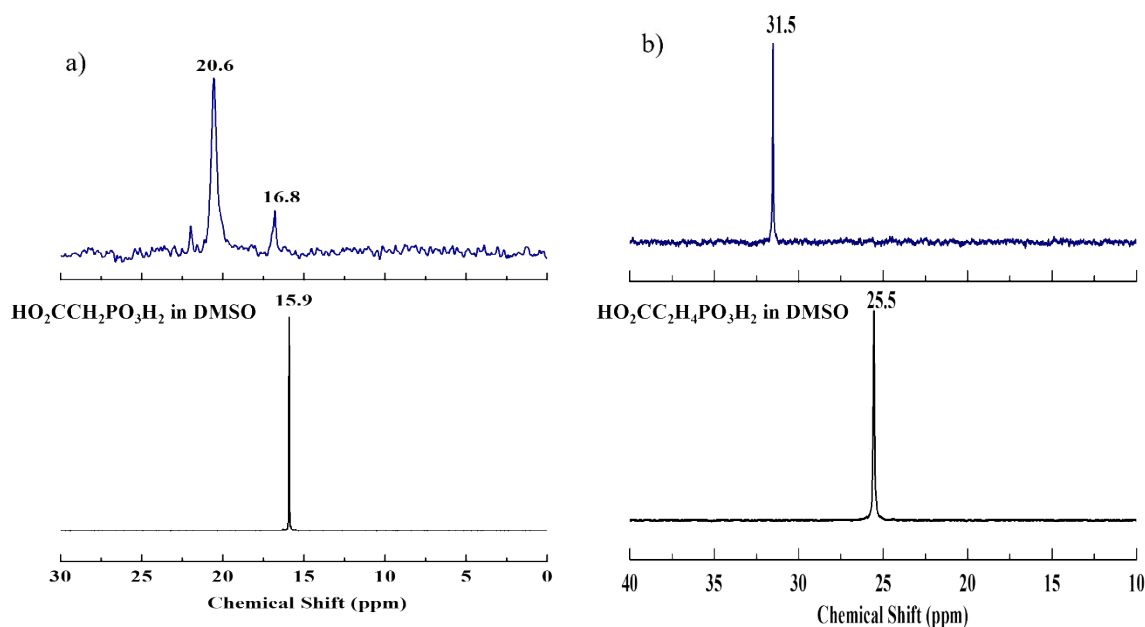


Figure S26. $^{31}\text{P}\{^1\text{H}\}$ NMR spectra of (a) $\text{NaNH}_4\text{-HO}_2\text{CCH}_2\text{PMo}_6$ (blue) and the neat hetero group $\text{HO}_2\text{CCH}_2\text{PO}_3\text{H}_2$ (black) as reference; (b) $\text{NaNH}_4\text{-HO}_2\text{CC}_2\text{H}_4\text{PMo}_6$ (blue) and the neat

hetero group $\text{HO}_2\text{CC}_2\text{H}_4\text{PO}_3\text{H}_2$ (black) as reference, dissolved in d_6 -DMSO at room temperature.

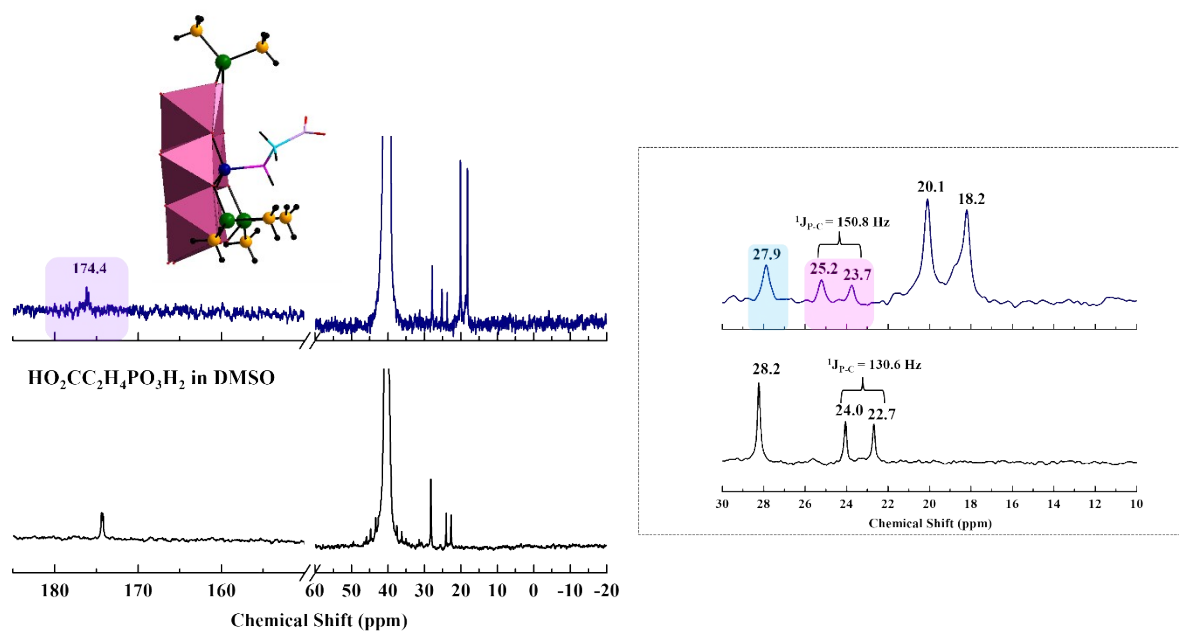


Figure S27. The figure illustrates the $^{13}\text{C}\{^1\text{H}\}$ NMR spectra of $\text{NaNH}_4\text{-HO}_2\text{CC}_2\text{H}_4\text{PMo}_6$ (blue) and the neat hetero group $\text{HO}_2\text{CC}_2\text{H}_4\text{PO}_3\text{H}_2$ (black) as reference, dissolved in d_6 -DMSO at room temperature. Peaks corresponding to structurally and hence magnetically inequivalent carbon atoms are labelled accordingly.

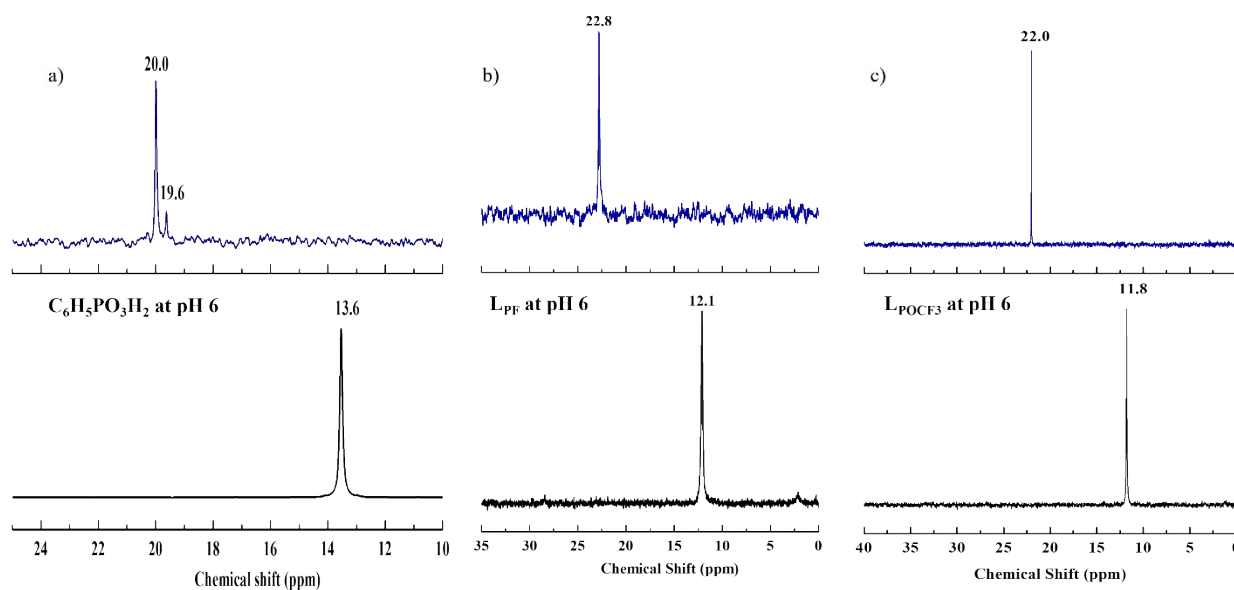
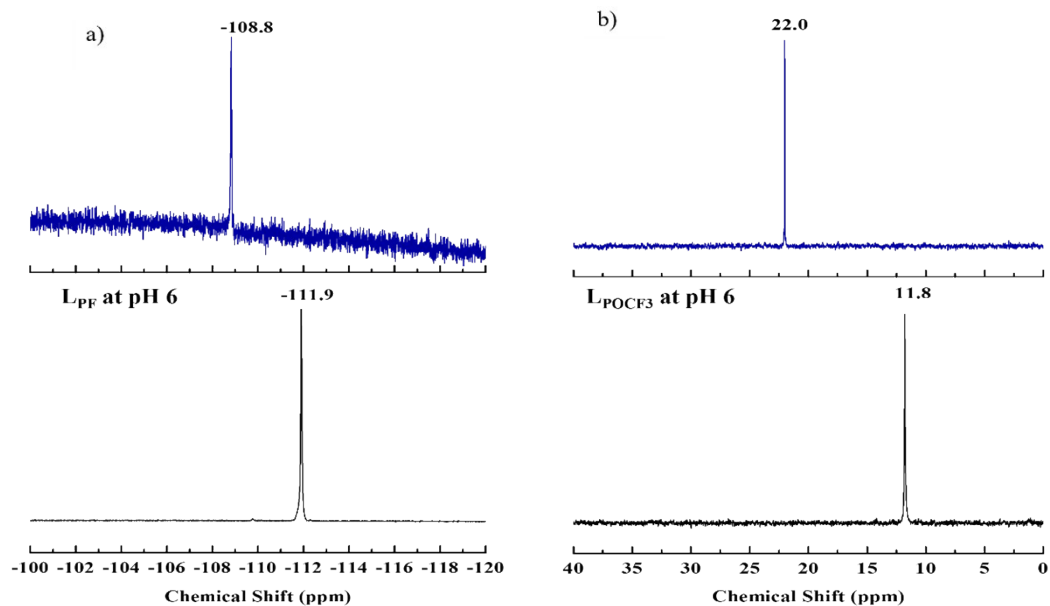


Figure S28. $^{31}\text{P}\{^1\text{H}\}$ NMR spectra of (a) $\text{NaNH}_4\text{-C}_6\text{H}_5\text{PMo}_6$ (blue) and the neat hetero group $\text{C}_6\text{H}_5\text{PO}_3\text{H}_2$ (black) as reference, dissolved in $d_6\text{-DMSO}$; (b) $\text{NaNH}_4\text{-FC}_6\text{H}_4\text{PMo}_6$ (blue) and the neat hetero group L_{PF} (black) as reference; (c) $\text{NaNH}_4\text{-F}_3\text{COC}_6\text{H}_4\text{PMo}_6$ (blue) and the neat hetero group L_{POCF_3} (black) as reference, dissolved in $\text{H}_2\text{O}/\text{D}_2\text{O}$ at room temperature.

Figure S29. ^{19}F NMR spectra of (a) $\text{NaNH}_4\text{-FC}_6\text{H}_4\text{PMo}_6$ (blue) and the neat hetero group L_{PF} (black) reference; (b) $\text{NaNH}_4\text{-F}_3\text{COC}_6\text{H}_4\text{PMo}_6$ (blue) and the neat hetero group L_{POCF_3} (black) as reference, dissolved in $\text{H}_2\text{O}/\text{D}_2\text{O}$ at room temperature.



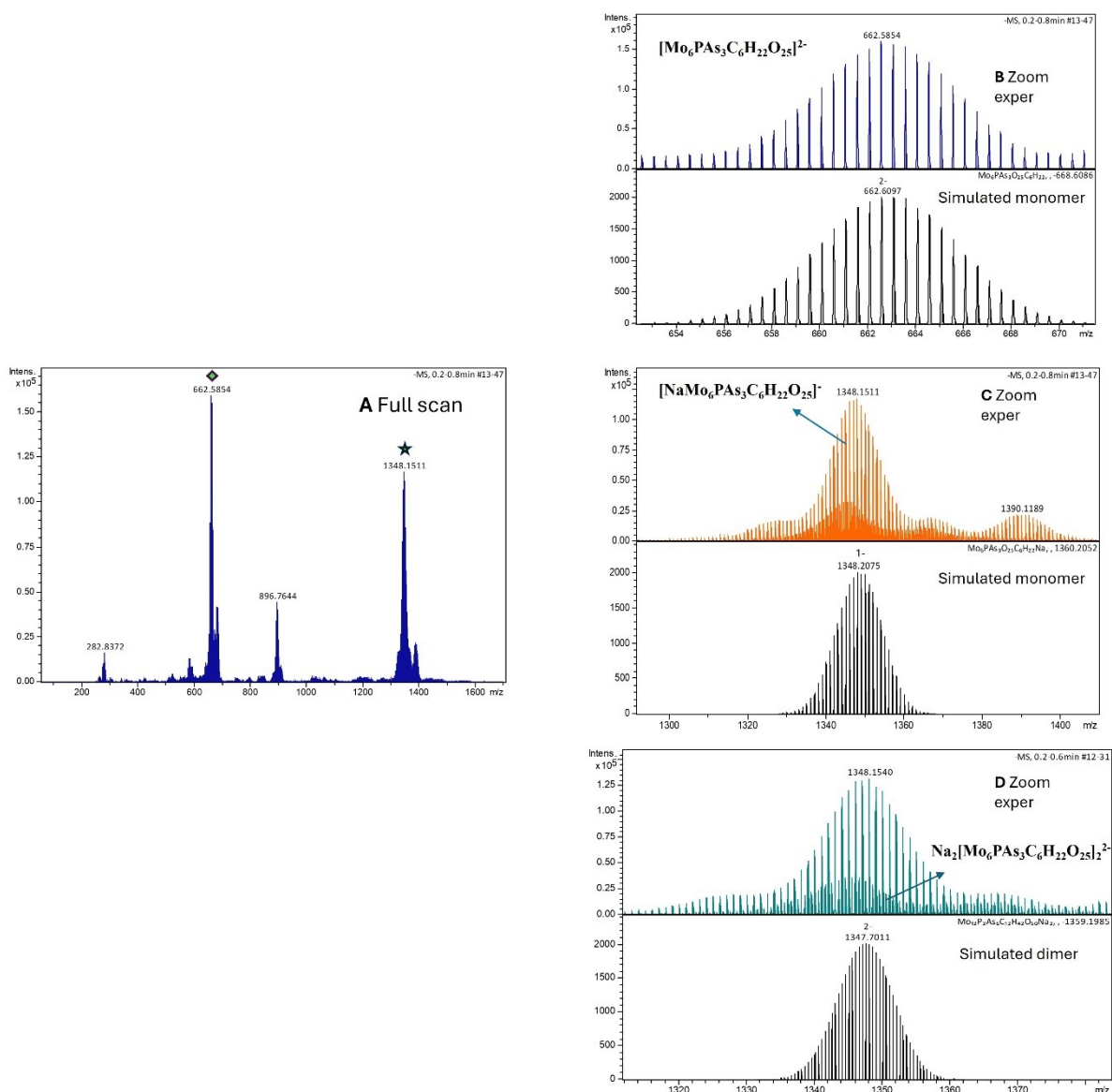


Figure S30: Negative mode ESI mass spectra of compound PMo_6 . **A:** Full scan full range view; **B:** expanded region around m/z 662 with experimental spectra in upper panel and simulated isotope pattern in bottom panel; **C:** expanded region around m/z 1348 with experimental spectra in upper panel (please note signals of dimeric species at lower intensity in between main signals) and simulated isotope pattern for the monomer in bottom panel; **D:** expanded region around m/z 1348 with experimental spectra in upper panel and simulated isotope pattern for the dimer in bottom panel.

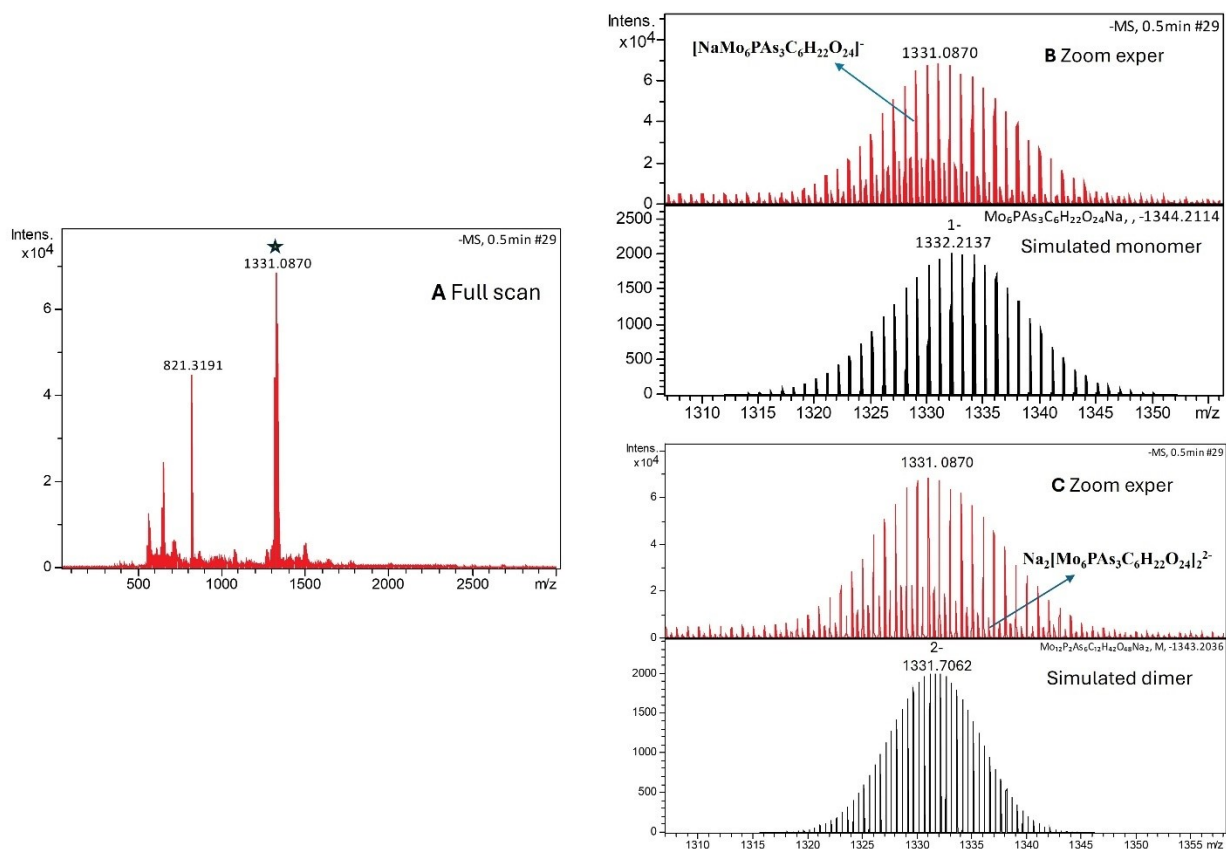


Figure S31. Negative mode ESI mass spectra of polyanion HPMo_6 . **A:** Full scan full range view; **B:** expanded region around m/z 1331 with experimental spectra in upper panel (please note signals of dimeric species at lower intensity in between main signals) and simulated isotope pattern for the monomer in bottom panel; **C:** expanded region around m/z 1331 with experimental spectra in upper panel and simulated isotope pattern for the dimer in bottom panel.

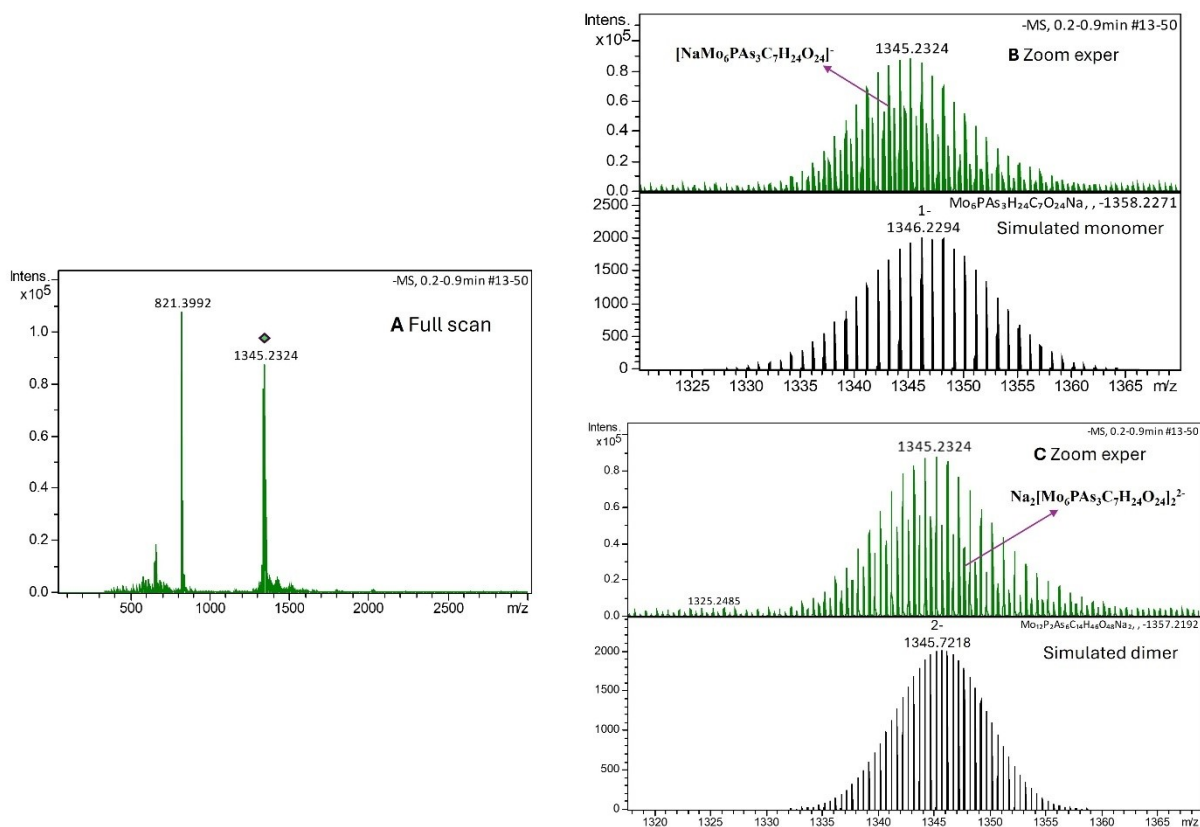


Figure S32. Negative mode ESI mass spectra of polyanion CH_3PMo_6 . **A:** Full scan full range view; **B:** expanded region around m/z 1345 with experimental spectra in upper panel (please note signals of dimeric species at lower intensity in between main signals) and simulated isotope pattern for the monomer in bottom panel; **C:** expanded region around m/z 1345 with experimental spectra in upper panel and simulated isotope pattern for the dimer in bottom panel.

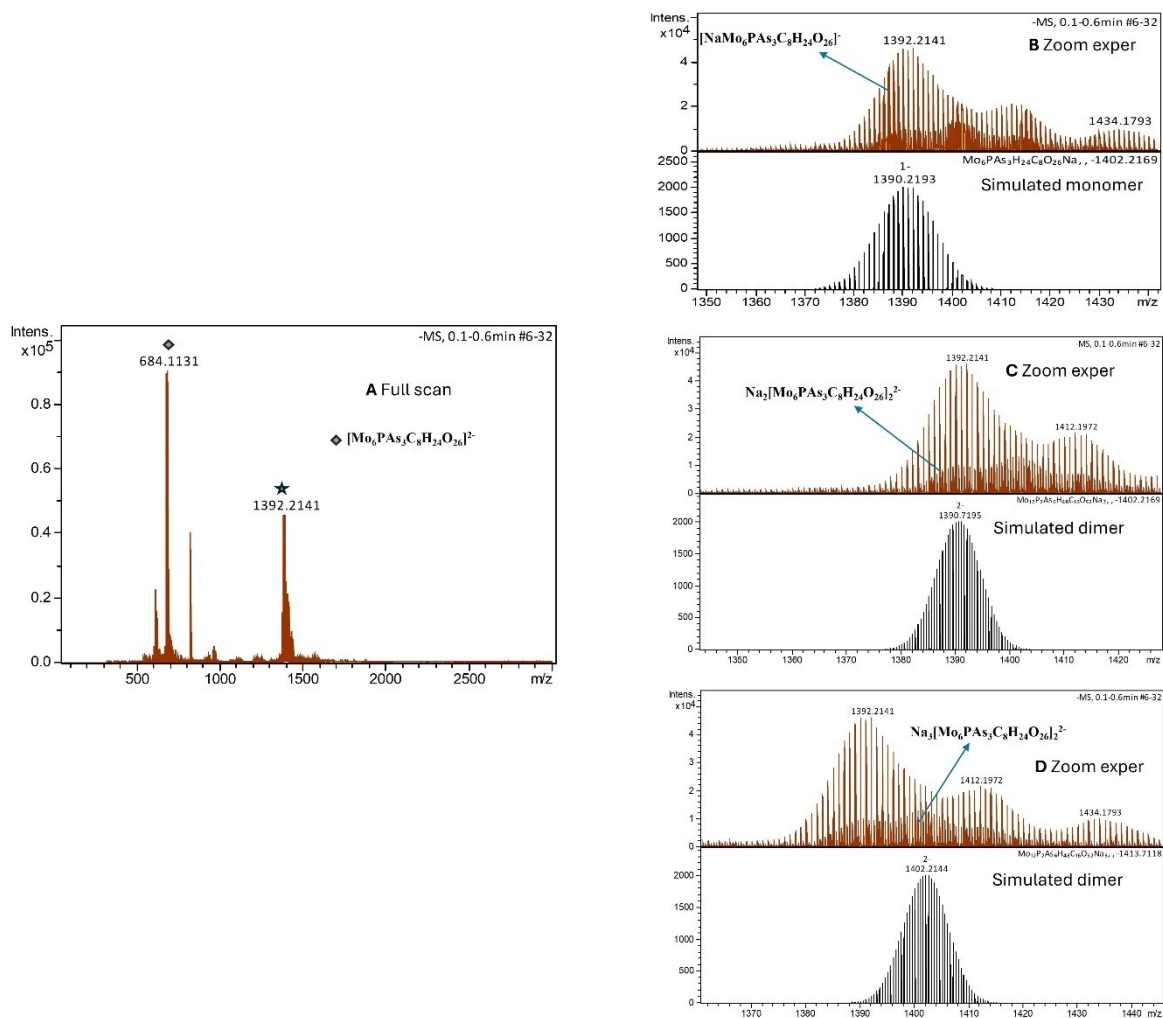


Figure S33. Negative mode ESI mass spectra of polyanion $\text{HO}_2\text{CCH}_2\text{PMo}_6$. **A:** Full scan full range view; **B:** expanded region around m/z 1345 with experimental spectra in upper panel (please note signals of dimeric species at lower intensity in between main signals) and simulated isotope pattern for the monomer in bottom panel; **C:** expanded region around m/z 1345 with experimental spectra in upper panel and simulated isotope pattern for the dimer in bottom panel; **D:** expanded region around m/z 1345 with experimental spectra in upper panel and simulated isotope pattern for the dimer in bottom panel.

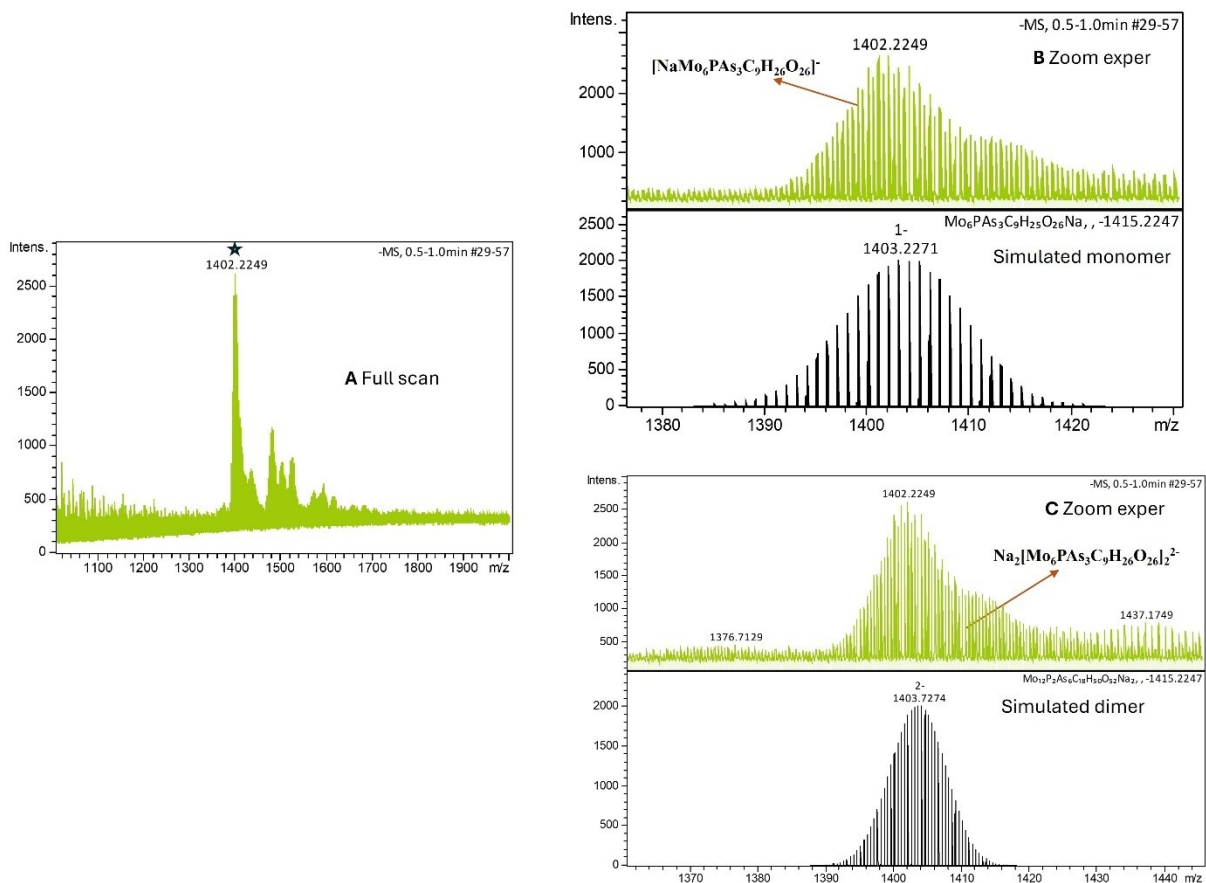


Figure S34. Negative mode ESI mass spectra of polyanion $\text{HO}_2\text{CC}_2\text{H}_4\text{PMo}_6$. **A:** Full scan full range view; **B:** expanded region around m/z 1402 with experimental spectra in upper panel (please note signals of dimeric species at lower intensity in between main signals) and simulated isotope pattern for the monomer in bottom panel; **C:** expanded region around m/z 1402 with experimental spectra in upper panel and simulated isotope pattern for the dimer in bottom panel.

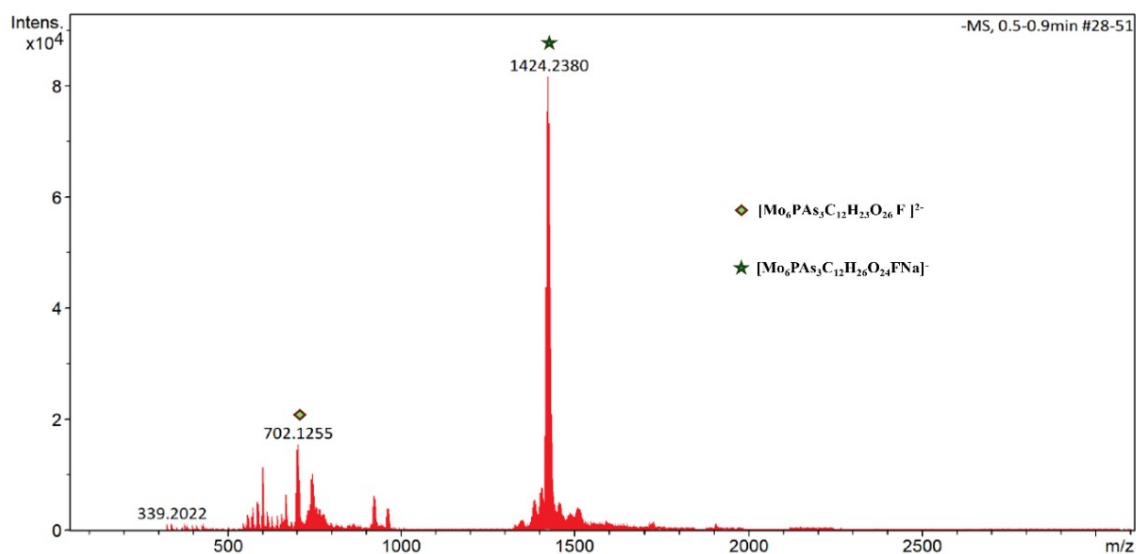


Figure S35. Negative mode ESI mass spectra of polyanion $4\text{-FC}_6\text{H}_4\text{PMo}_6$. **A:** Full scan full range view.

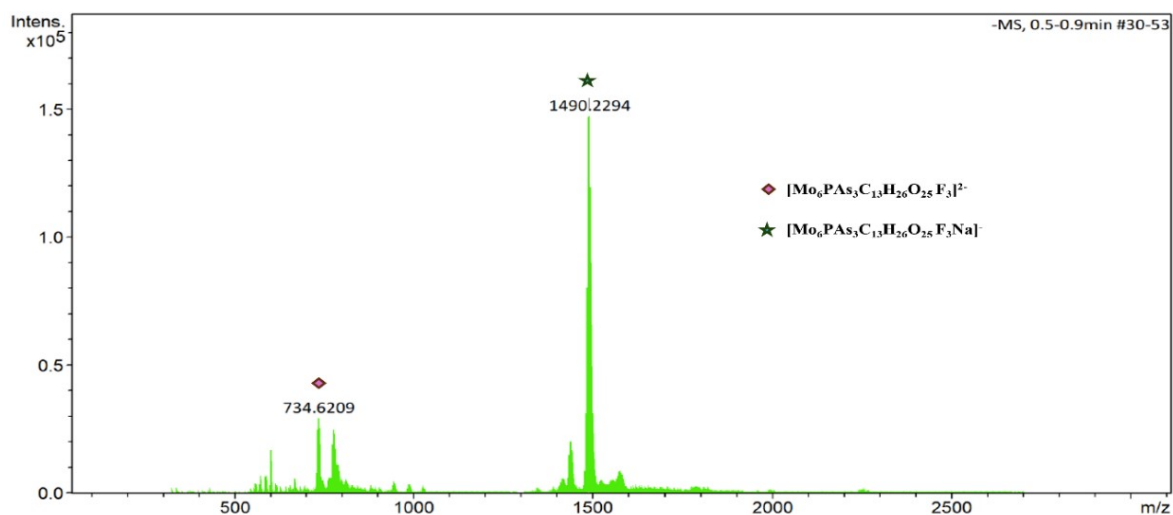


Figure S36. Negative mode ESI mass spectra of polyanion **4-F₃COC₆H₄PMo₆**. **A:** Full scan full range view.

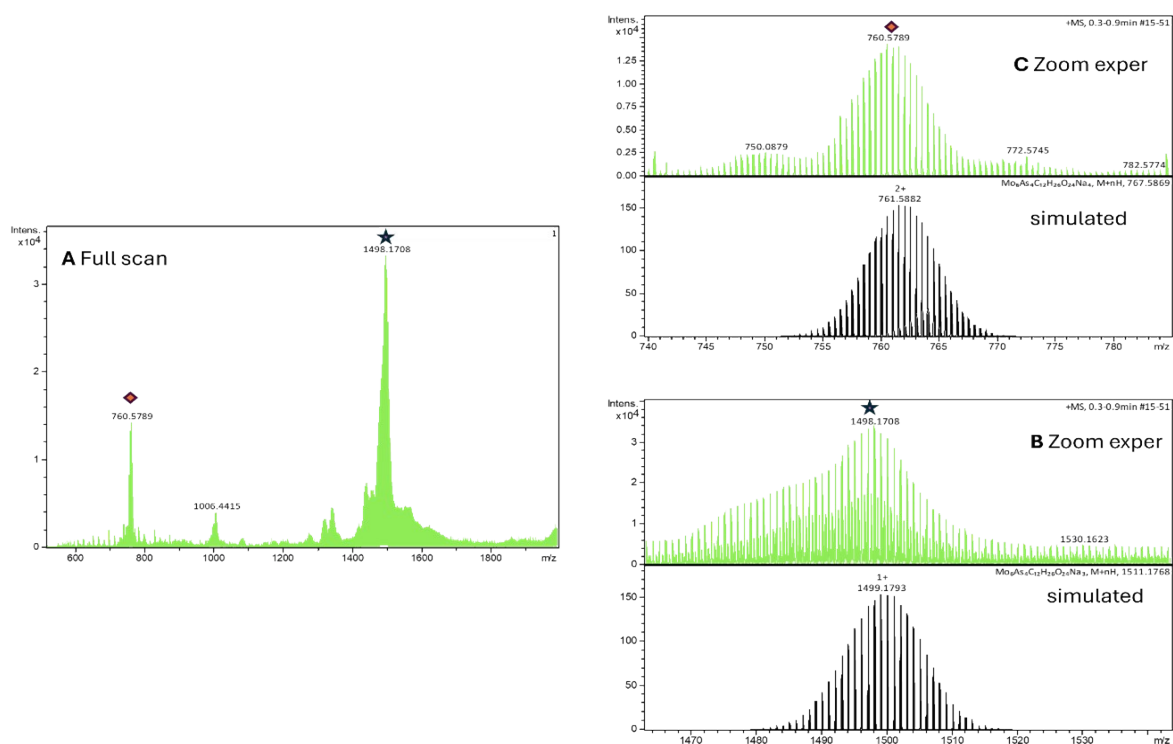


Figure S37. Positive mode ESI mass spectra of polyanion **Mo₇**. **A:** Full scan full range view; **B:** expanded region around m/z 1498 with experimental spectra in upper panel and simulated isotope pattern in bottom panel; **C** expanded region around m/z 760.5 with experimental spectra in upper panel and simulated isotope pattern in bottom panel.

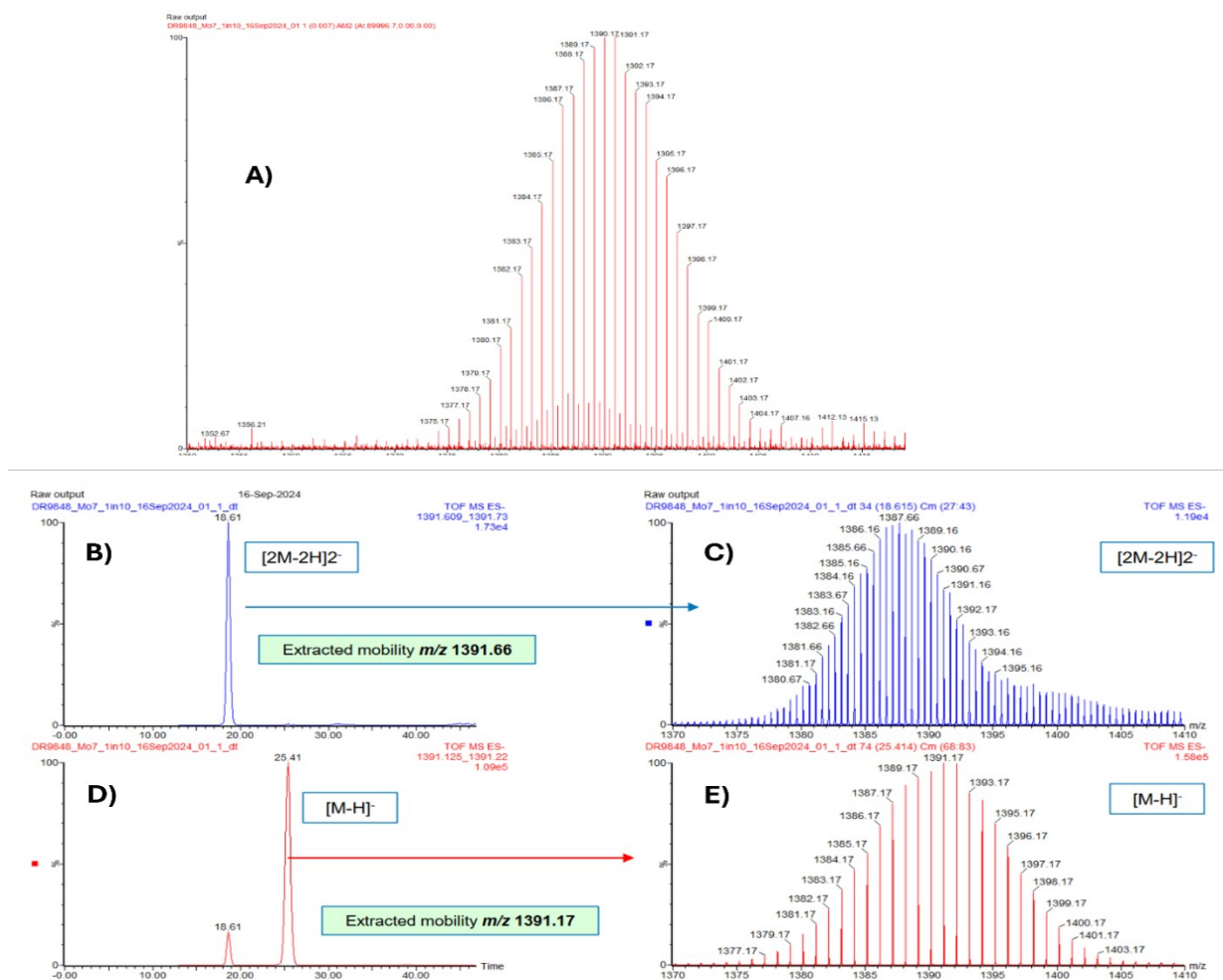


Figure S38. Negative mode ESI ion mobility mass spectra of polyanion Mo_7 and corresponding mobilograms. **A:** Expanded view of ESI mass spectrum with two overlapping species; **B:** Extracted ion mobilogram of m/z 1391.7 showing single dimeric species $[2\text{M}-2\text{H}]^{2-}$; **C:** ESI mass spectrum corresponding to dimeric species $[2\text{M}-2\text{H}]^{2-}$; **D:** Extracted ion mobilogram of m/z 1391.2 showing single monomeric species $[\text{M}-\text{H}]^-$; **E:** ESI mass spectrum corresponding to monomeric species $[\text{M}-\text{H}]^-$.